Research Paper

Long non-coding RNA, HOTAIRM1, promotes glioma malignancy by forming a ceRNA network

Qingyu Liang[1], Xue Li[1], Gefei Guan[1], Xiaoyan Xu[2], Chen Chen[3], Peng Cheng[1], Wen Cheng[1], Anhua Wu[1]

[1]Department of Neurosurgery, The First Hospital of China Medical University, Shenyang, Liaoning Province, China
[2]Department of Pathophysiology, College of Basic Medicine Science, China Medical University, Shenyang, Liaoning Province, China
[3]The Research Center for Medical Genomics, Key Laboratory of Cell Biology, Ministry of Public Health, Key Laboratory of Medical Cell Biology, Ministry of Education, College of Life Sciences, China Medical University, Shenyang, Liaoning Province, China

Correspondence to: Anhua Wu, Wen Cheng; **email:** wuanhua@yahoo.com, cmu071207@163.com
Keywords: glioma, HOTAIRM1, prognosis, ceRNA network, immune microenvironment
Received: April 30, 2019 **Accepted:** August 12, 2019 **Published:** September 2, 2019

ABSTRACT

Long non-coding RNAs play critical roles in tumorigenesis and the immune process. In this study, RNA sequencing data for 946 glioma samples from The Cancer Genome Atlas and the Chinese Glioma Genome Atlas databases were analyzed to evaluate the prognostic value and function of homeobox A transcript antisense RNA myeloid-specific (HOTAIRM)1. HOTAIRM1 expression was associated with clinical and molecular features of glioma: patients with high HOTAIRM1 expression were more likely to be classified as malignant cases, and elevated HOTAIRM1 level was associated with shorter survival time in subgroups stratified by clinical and molecular features. A multivariate Cox regression analysis showed that HOTAIRM1 was an independent prognostic factor for patient outcome. In vitro experiments revealed that HOTAIRM1 knockdown suppressed the malignant behavior of glioma and increased tumor sensitivity to temozolomide. The results of an in silico analysis indicated that HOTAIRM1 promotes the malignancy of glioma by acting as a sponge for microRNA (miR)-129-5p and miR-495-3p. HOTAIRM1 overexpression was also associated with immune activation characterized by enhanced T cell-mediated immune and inflammatory responses. These results suggest that HOTAIRM1 is a prognostic biomarker and potential therapeutic target in glioma.

INTRODUCTION

Glioma is the most prevalent and lethal primary brain tumor, accounting for nearly 30% of all cases [1]. Patients with glioma—especially glioblastoma multiforme (GBM)—have poor prognosis, with a median survival of approximately 14 months, even with treatment (surgery, radiotherapy, and adjuvant chemotherapy) [2, 3]. Several studies have examined the molecular mechanisms underlying glioma malignancy and identified promising therapeutic targets [3, 4]; however, the possibility of predicting prognosis and treatment effects in glioma is limited.

Long non-coding (lnc)RNAs, which are ncRNAs that are longer than 200 bases in length [5], are frequently found to be dysregulated in tumors. The lncRNA homeobox (HOX)A transcript antisense RNA (HOTAIR) located between the HOXC11 and HOXC12 loci is marker for glioma and other solid tumors [6]. HOTAIR promotes tumor progression by acting as a micro (mi)RNA sponge [7] and promoting an immunosuppressive tumor microenvironment [8].

HOTAIR myeloid-specific (HOTAIRM)1 is a lncRNA located between the HOXA1 and HOXA2 loci that was first identified as a myeloid-specific regulator of

the HOXA gene family, which controls target gene transcription through chromosome remodeling during myeloid cell differentiation and maturation [9]. HOTAIRM1 functions as a tumor suppressor in colorectal, head and neck, gastric, and lung cancers by sponging micro (mi)RNAs and regulating immunosuppressive myeloid-derived suppressor cells [10–13]. However, HOTAIRM1 was also shown to promote cell proliferation and migration in pancreatic ductal adenocarcinoma [14]. Therefore, additional studies are needed to clarify the role of HOTAIRM1 in cancer.

To this end, in the present study we investigated the clinical relevance of HOTAIRM1 overexpression by analyzing 946 glioma specimens in The Cancer Genome Atlas (TCGA) and the Chinese Glioma Genome Atlas (CGGA) databases. We also examined the function of HOTAIRM1 by gene silencing in glioma cell lines. The results indicate that HOTAIRM1 plays an important role in the malignancy of glioma and is a potential therapeutic target for its treatment.

RESULTS

Association between HOTAIRM1 expression and clinical and molecular features of glioma

Samples from the TCGA and CGGA datasets were arranged according to increasing HOTAIRM1 expression level and the association between HOTAIRM1 expression and clinical and molecular features of glioma was examined (Figure 1A). Age at diagnosis was positively correlated with HOTAIRM1 level (Figure 1A and Supplementary Figure 1A, 1J). High HOTAIRM1 expression was frequently observed in patients with low Karnofsky Performance Score (KPS; Supplementary Figure 1A); these patients were more likely to exhibit a malignant phenotype (Figure 1A) and harbor wild-type alpha thalassemia/mental retardation syndrome X-linked (ATRX), isocitrate dehydrogenase (IDH), and telomerase reverse transcriptase promoter; mutant phosphatase and tensin homolog (PTEN), tumor protein (TP)53, and epidermal growth factor receptor (EGFR); and exhibit O-6-methylguanine-DNA methyltransferase (MGMT) promoter demethylation,1p/19q non-codeletion, and Chr7 gain/Chr10 loss (Figure 1A and Supplementary Figure 1A–1I and 1K–1O).

We compared clinical and molecular features between patients with high and low HOTAIRM1 expression and found that World Health Organization (WHO) grade, histopathology, IDH mutation status, MGMT promoter methylation status, and 1p/19q co-deletion status were associated with HOTAIRM1 level (Supplementary Table 3). Thus, HOTAIRM1 expression is correlated with clinical and molecular features of glioma.

HOTAIRM1 is positively associated with glioma malignancy

To determine the relationship between HOTAIRM1 expression and glioma malignancy, we analyzed the association between HOTAIRM1 level and WHO grade and molecular classification. HOTAIRM1 overexpression was positively correlated with grade progression in TCGA specimens (Figure 1B). Of the five previously established molecular classifications [15], higher HOTAIRM1 expression was more frequently detected in low-grade glioma (LGG) with wild-type IDH (LGG-IDHwt) and GBM with wild-type IDH cases (Figure 1B). In terms of TCGA molecular subtypes, HOTAIRM1 expression was higher in the mesenchymal subtype than in the proneural subtype (Figure 1B and Supplementary Table 4). Analysis of the CGGA dataset yielded similar findings (Figure 1C and Supplementary Table 4).

We next examined HOTAIRM1 expression in an independent glioma cohort (Grade II, n = 10, Grade III, n = 10, and Grade IV, n = 8), four non-neoplastic brain tissue specimens, five glioma cell lines, one normal astrocyte cell line, and three primary glioma cell lines [differentiated glioblastoma cells (DGCs)] derived from glioma patients. Consistent with the above results, high HOTAIRM1 expression was associated with higher malignancy in these samples (Figure 1D, 1E), indicating that HOTAIRM1 overexpression is linked to glioma malignancy.

High HOTAIRM1 expression predicts reduced survival of glioma patients

To determine the association between HOTAIRM1 expression and overall survival (OS) of glioma patients, we dichotomized median HOTAIRM1 levels into high expression (high-exp) and low expression (low-exp) groups. OS was shorter in the high-exp group compared to the low-exp group (median OS = 21.3 vs. 106.7 months, $P < 0.0001$; Figure 2A). We also examined the prognostic value of HOTAIRM1 in stratified groups (Grades II, III, and IV) and observed similar trends in the Kaplan–Meier survival curves (Figure 2A–2D). These results were confirmed in the CGGA dataset (Figure 2E–2H).

To assess the prognostic value of HOTAIRM1 in the stratified cohorts, patients were classified according to clinical factors (age, KPS, radiation, and chemotherapy) and genomic aberrations (IDH and ATRX mutation, MGMT promoter methylation, and 1p/19q

co-deletion status). In most cohorts, high-exp patients had significantly shorter OS than those in the low-exp group (Figure 3A–3T and Supplementary Figure 2A, 2B) and tended to have poor prognosis, although the results were non-significant. We also examined the independence of HOTAIRM1 in the two datasets by Cox regression analysis. Uni- and multivariate analyses suggested that HOTAIRM1 is an independent prognostic factor in glioma [hazard ratio (HR) = 2.0559, P = 0.0042 in TCGA; HR = 2.6894, P < 0.0001 in CGGA; Table 1].

The predictive value of HOTAIRM1 for 1-, 3-, and 5-year survival in TCGA and CGGA datasets was evaluated based on a receiver operating characteristic curve. The area under the curve for 1-, 3-, and 5-year survival was 74.56%, 75.87%, and 77.65%, respectively,

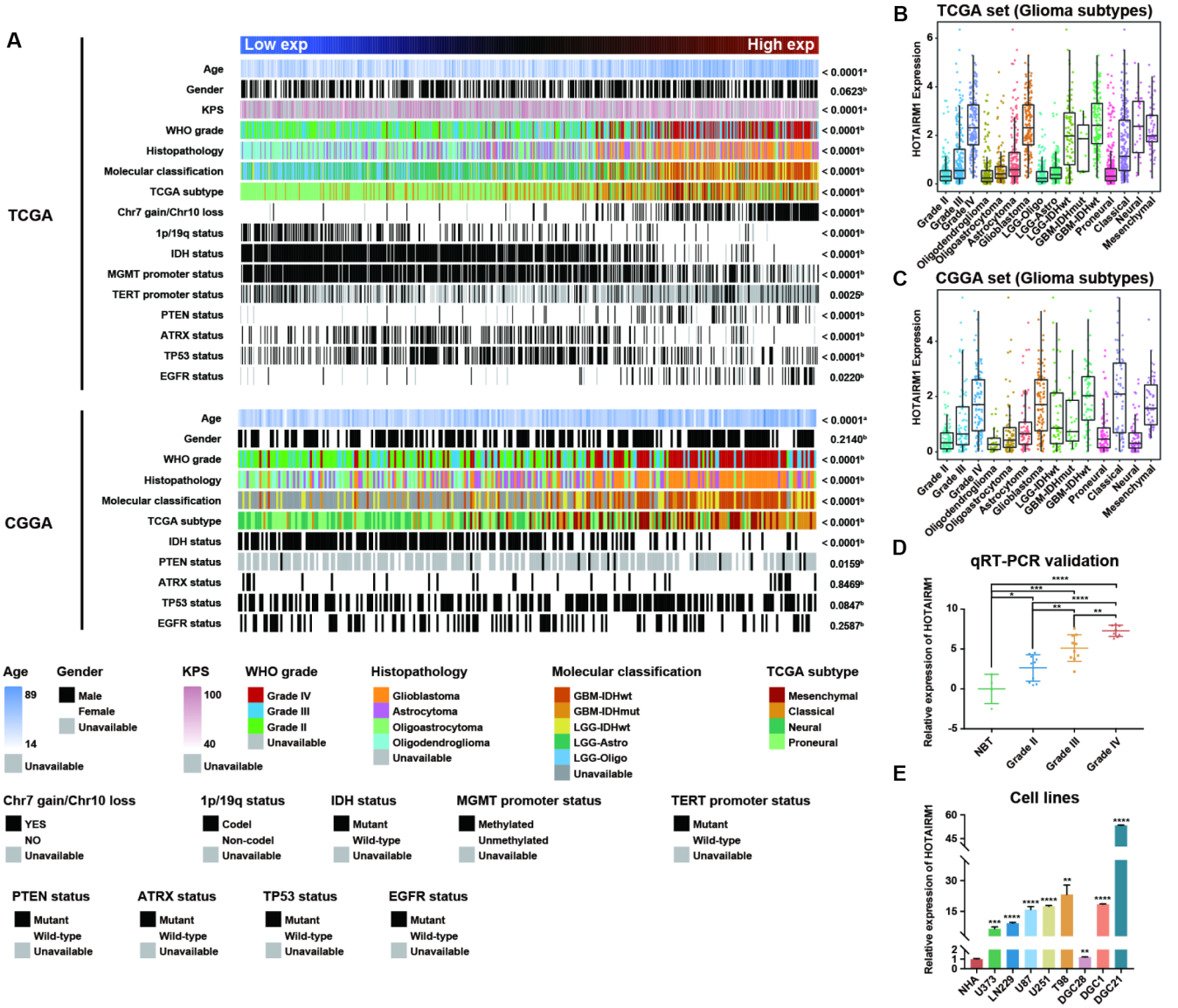

Figure 1. Association between HOTAIRM1 expression and clinical and molecular features and malignancy in glioma. (**A**) TCGA (top) and CGGA (bottom) data were arranged in ascending order of HOTAIRM1 expression level; the relationship between HOTAIRM1 level and clinical and molecular features of glioma was evaluated. a, Difference in continuous variables between high- and low-exp groups was assessed with the Student's t test; b, distribution of categorical variables between high- and low-exp groups was assessed with the χ^2 test or Fisher's exact test. (**B**, **C**) HOTAIRM1 expression level according to tumor grade, histopathologic classification, and molecular and TCGA subtypes in TCGA (B) and CGGA (**C**). (**D**, **E**) qRT-PCR analysis of relative HOTAIRM1 expression level in four non-neoplastic brain tissue samples, 28 glioma tissue samples (Grade II, n = 10, Grade III, n = 10, and Grade IV, n = 8), normal human astrocytes (NHA), five glioma cell lines, and three primary DGC lines derived from glioma patients. Values represent mean ± SD. *P < 0.05, **P < 0.01, ***P < 0.001, ****P < 0.0001 (Student's t test).

in TCGA and 69.51%, 76.49%, and 76.89%, respectively, in CGGA. Thus, HOTAIRM1 is a better predictor of glioma patient survival than age, tumor grade, IDH mutation status, chemotherapy, and radiotherapy (Supplementary Figure 3A–3F).

Functional analysis of HOTAIRM1 in glioma

Gene expression profiles were analyzed to examine the phenotypes associated with HOTAIRM1 overexpression. TCGA data were used as the discovery set and CGGA data were used for validation in the whole-transcriptome principal components analysis (PCA). We found that patients with high and low HOTAIRM1 expression had distinct transcriptome profiles (Supplementary Figure 4A, 4B). Differentially expressed genes (DEGs) that were significantly upregulated (up-DEGs) in the high-exp group (log2 fold change > 2, $P < 0.05$; Supplementary Dataset 1) were associated with malignant tumor behavior and immune and inflammatory responses—e.g., collagen catabolism, wound healing, positive regulation of cell proliferation, cell adhesion, inflammatory response, cellular response to tumor necrosis factor, chemokine-mediated signaling, neutrophil chemotaxis, monocyte chemotaxis, response to lipopolysaccharide, acute-phase response, and immune response (Figure 4A, 4B). These results were validated by gene set enrichment analysis (GSEA) (Figure 4C–4H and Supplementary Figure 4C–4N).

HOTAIRM1 promotes glioma proliferation and invasion in vitro

Small interfering (si)RNA-mediated knockdown of HOTAIRM1 expression in the U87 and LN229 glioma cell lines decreased HOTAIRM1 transcript level 48 h later (Supplementary Figure 5A). The results of the Cell Counting Kit (CCK)-8 assay showed that HOTAIRM1 silencing suppressed the proliferation of U87 and LN229 cells (Figure 5A), which was accompanied by decreased cell migration and invasion (Figure 5B and Supplementary Figure 5B). Thus, HOTAIRM1 has an oncogenic function in glioma.

HOTAIRM1 promotes epithelial–mesenchymal transition (EMT) and temozolomide (TMZ) resistance

We performed PCA to investigate the functional significance of HOTAIRM1 overexpression in glioma. The results showed that high- and low-exp groups expressed distinct EMT gene sets, which was confirmed by GSEA (Supplementary Figure 6A, 6B). HOTAIMR1 knockdown increased E-cadherin and decreased vimentin protein levels relative to the control group (Figure 5C) and after 10 days, altered the morphology of U87 cells to a cobblestone-like appearance suggestive of mesenchymal-to-epithelial transition (Supplementary Figure 6C).

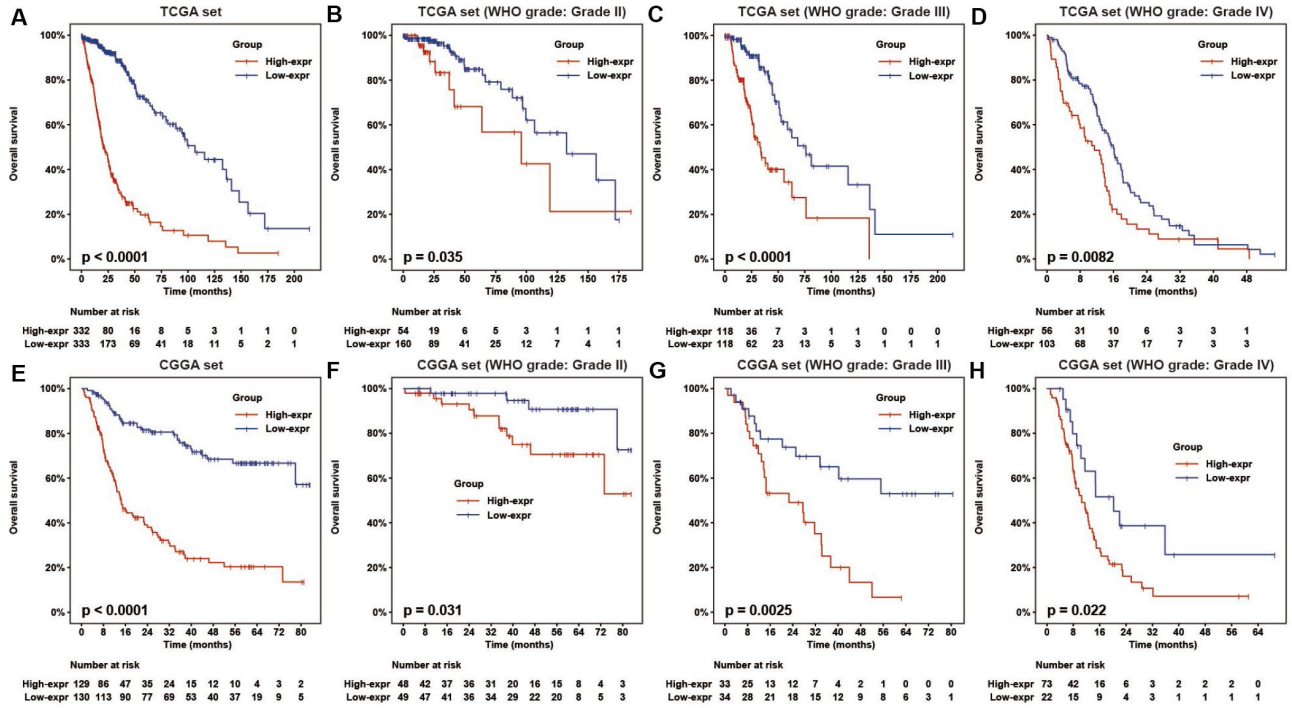

Figure 2. HOTAIRM1 expression is correlated with glioma patient prognosis. (**A–H**) Prognostic value of HOTAIRM1 in all cases (**A**, **E**) and according to glioma grade (**B–D**, **F–H**).

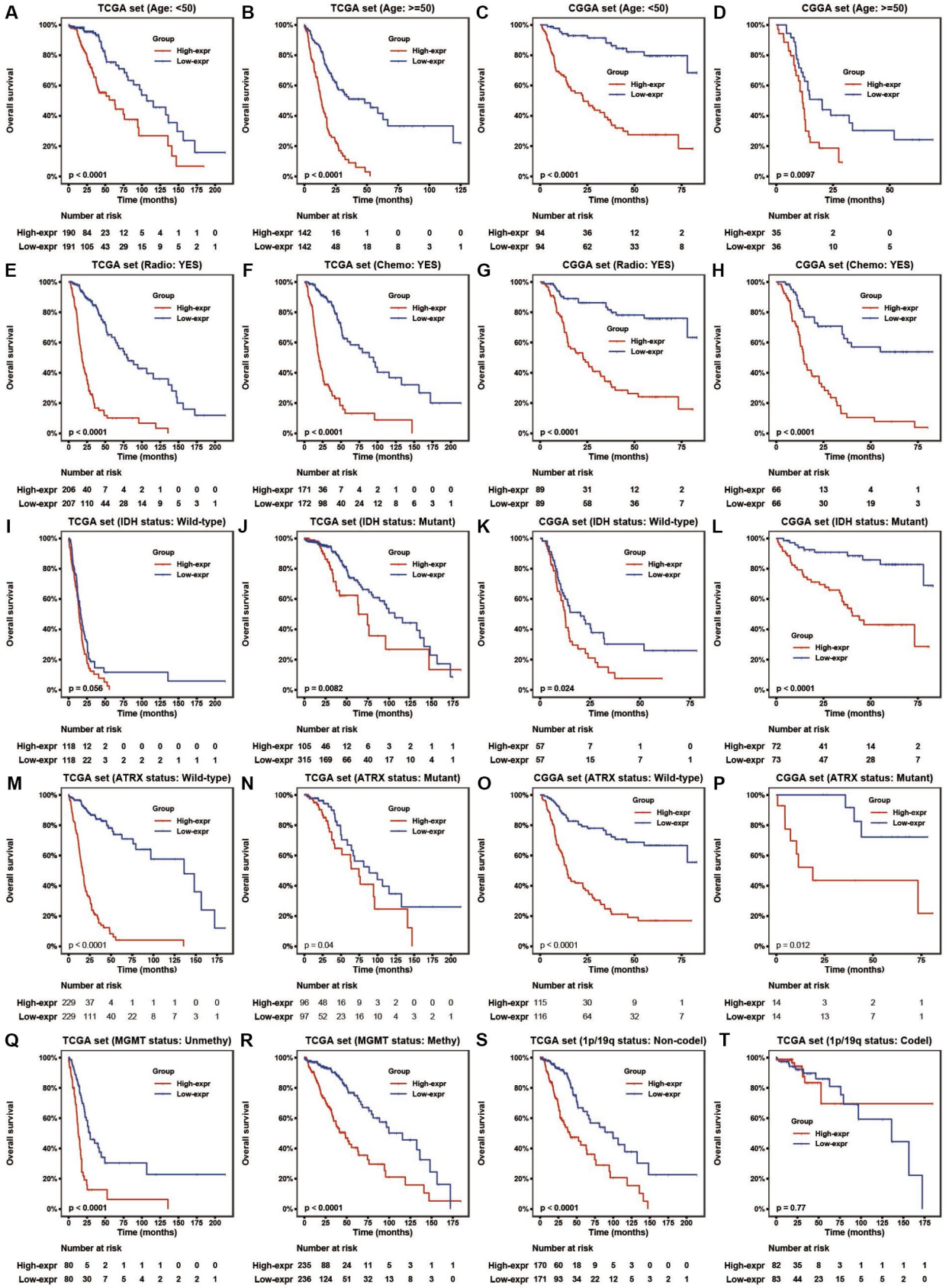

Figure 3. HOTAIRM1 maintains high prognostic value in stratified groups. (**A**–**T**) Prognostic value of HOTAIRM1 in TCGA and CGGA cohorts stratified by clinical (**A**–**H**) and genomic (**I**–**T**) features.

Table 1. Uni- and multivariate Cox analyses of prognostic factors in glioma.

Variable	TCGA set					CGGA set				
	Number of samples	Univariate		Multivariate		Number of samples	Univariate		Multivariate	
		p value	HR	p value	HR		p value	HR	p value	HR
Age										
Increasing years	670	<0.0001	1.0672	<0.0001	1.0405	274	<0.0001	1.0391	0.4957	0.9927
Gender										
Female vs Male	670	0.1456	0.8271			274	0.2944	0.8165		
WHO Grade										
Grade IV	160	ref.	ref.	ref.	ref.	101	ref.	ref.	ref.	ref.
Grade III	237	<0.0001	0.1496	0.0047	0.5426	72	<0.0001	0.3752	0.1054	0.6731
Grade II	216	<0.0001	0.1422	<0.0001	0.2554	101	<0.0001	0.0696	<0.0001	0.1109
Radiotherapy										
Yes vs No	611	0.0001	1.9199	0.0120	0.5843	255	0.0002	0.4646	0.0001	0.4274
Chemotherapy										
Yes vs No	396	0.0008	0.5529			248	0.0079	1.6935	0.0502	0.6420
Chr7 gain/Chr10 loss										
YES vs NO	663	<0.0001	8.1843	0.3358	1.2242	Unavailable	Unavailable	Unavailable	Unavailable	Unavailable
1p/19q status										
Codel vs Noncodel	666	<0.0001	0.2199	0.0803	0.5071	Unavailable	Unavailable	Unavailable	Unavailable	Unavailable
IDH status										
Mutation vs Wild-type	663	<0.0001	0.0993	0.0664	0.5265	274	<0.0001	0.2353	0.0854	0.6269
ATRX status										
Mutation vs Wild-type	658	<0.0001	0.4201	0.9901	0.9961	274	0.2168	0.6757		
MGMT promoter status										
Methylated vs Unmethylated	638	<0.0001	0.3022	0.1081	0.7417	Unavailable	Unavailable	Unavailable	Unavailable	Unavailable
HOTAIRM1										
High- vs Low-exp	672	<0.0001	5.8674	0.0042	2.0559	274	<0.0001	4.3906	0.0001	2.6894

Given that EMT is associated with drug resistance, we explored the relationship between HOTAIRM1 expression and patient prognosis under different treatments. In patients who received radio- or chemotherapy, elevated HOTAIRM1 level was an indicator of poor prognosis (Figure 3E–3H). Additionally, patients in the low-exp group who received radiochemotherapy had longer OS than those treated with radiation alone, but this was not observed in patients with high HOTAIRM1 expression (Figure 5D). The results of the chemo-sensitivity assay showed that HOTAIRM1 knockdown in U87 and LN229 cells increased sensitivity to TMZ treatment, as evidenced by a 2-fold decrease in the half-maximal inhibitory concentration (IC50) of TMZ (Supplementary Table 5).

Establishment of a HOTAIRM1–miRNA–mRNA network

Several lncRNAs act as a competing endogenous (ce)RNAs for miRNAs [16]. To investigate whether HOTAIRM1 has this function, putative target miRNAs of HOTAIRM1 in an online database were identified using DIANA tools and LncBase Predicted v.2. Three miRNAs that were downregulated in GBM compared with normal brain tissue ($P < 0.01$; Supplementary Dataset 2)—i.e., hsa-miR-129-5p, hsa-miR-495-3p, and hsa-miR-539-5p—were selected for further analysis (Figure 6A). We identified 3137 target genes of these three miRNAs in starBase v.3.0. Genes in the overlap between miRNA targets and up-DEGs were screened (754 genes; Supplementary Dataset 1), yielding a set of 51 genes for further analysis (Figure 6B).

We constructed a lncRNA–miRNA–mRNA (i.e., ceRNA) network (Figure 6C) to gain insight into the relationship between HOTAIRM1, its target miRNAs, and up-DEGs. A protein–protein interaction (PPI) network was developed to evaluate interactions among the 51 target genes (Figure 7A). The Molecular Complex Detection (MCODE) approach was used to identify hub genes from the PPI network. Using k-core = 2 and degree cutoff = 3, we identified a sub-network containing 13 nodes and 31 edges (Figure 7B). A HOTAIRM1–miRNA–hub gene network was established to determine the association between HOTAIRM1, miRNAs, and hub genes (Figure 7C). The network had 15 lncRNA–miRNA–mRNA regulatory axes comprising HOTAIRM1, two miRNAs

(hsa-miR-129-5p and hsa-miR-495-3p), and 13 hub genes. Gene Ontology (GO) analysis of the hub genes using ClueGO showed that most of the biological functions were enriched in cytoskeleton and cell differentiation, which play an important role in cell migration and invasion (Figure 7C). We also analyzed the hsa-miR-129-5p and hsa-miR-495-3p binding sites in HOTAIRM1 and hub gene transcripts (Figure 7E and Supplementary Figure 7) and determined with a luciferase reporter assay that both hsa-miR-129-5p and hsa-miR-495-3p directly bind to HOTAIRM1 (Figure 7E); furthermore, both were upregulated by HOTAIRM1 knockdown (Figure 7F). Conversely, suppression of HOTAIRM1 decreased the expression of 12 of the 13 hub genes that were upregulated in the high-exp group (Figure 7D, 7F). However, in HOTAIRM1-depleted U87 and LN229 cells, only insulin-like growth factor-binding protein (IGFBP)3, collagen type I α2 chain, and superoxide dismutase (SOD)2 levels were restored by hsa-miR-495-3p inhibition whereas Forkhead box A1, collagen type III α1 chain, and collagen type V α1 chain levels were restored by inhibiting hsa-miR-129-5p. These data suggest that HOTAIRM1 functions as a ceRNA to promote glioma cell migration and invasion.

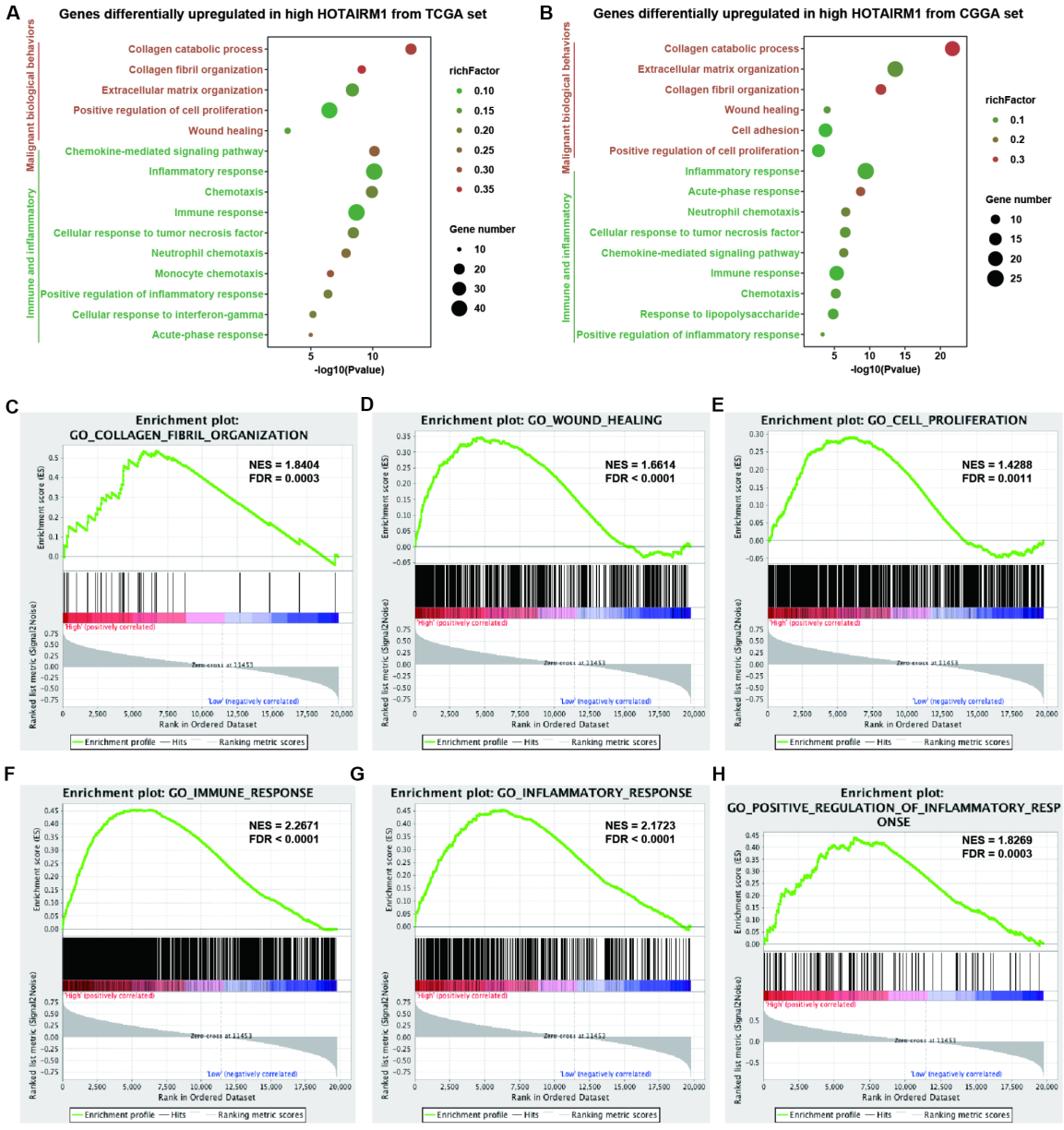

Figure 4. Analysis of HOTAIRM1 function in glioma. (**A**, **B**) GO analysis by DAVID showing biological processes associated with HOTAIRM1 in TCGA (**A**) and CGGA (**B**) datasets. (**C–H**) GSEA analysis was performed to verify the biological functions attributed to HOTAIRM1 in TCGA.

High HOTAIRM1 expression is associated with a distinct immune and inflammatory phenotype

GO analyses revealed that immune response and inflammatory activity in glioma were influenced by HOTAIRM1 level (Figure 4A, 4B). Some of the above-mentioned hub genes, including secreted phosphoprotein (SPP)1, IGFBP3, SOD2, and fibroblast growth factor 7 are involved in the regulation of the tumor immune response [17–20]. We examined the relationship between HOTAIRM1 and local immune status by performing PCA of gene sets related to immune activation, T cell-mediated immune response, and immune response to tumor cells extracted from Molecular Signatures Database v.6.2 (http://software.broadinstitute.org/gsea/index.jsp; Supplementary Dataset 3). The results showed

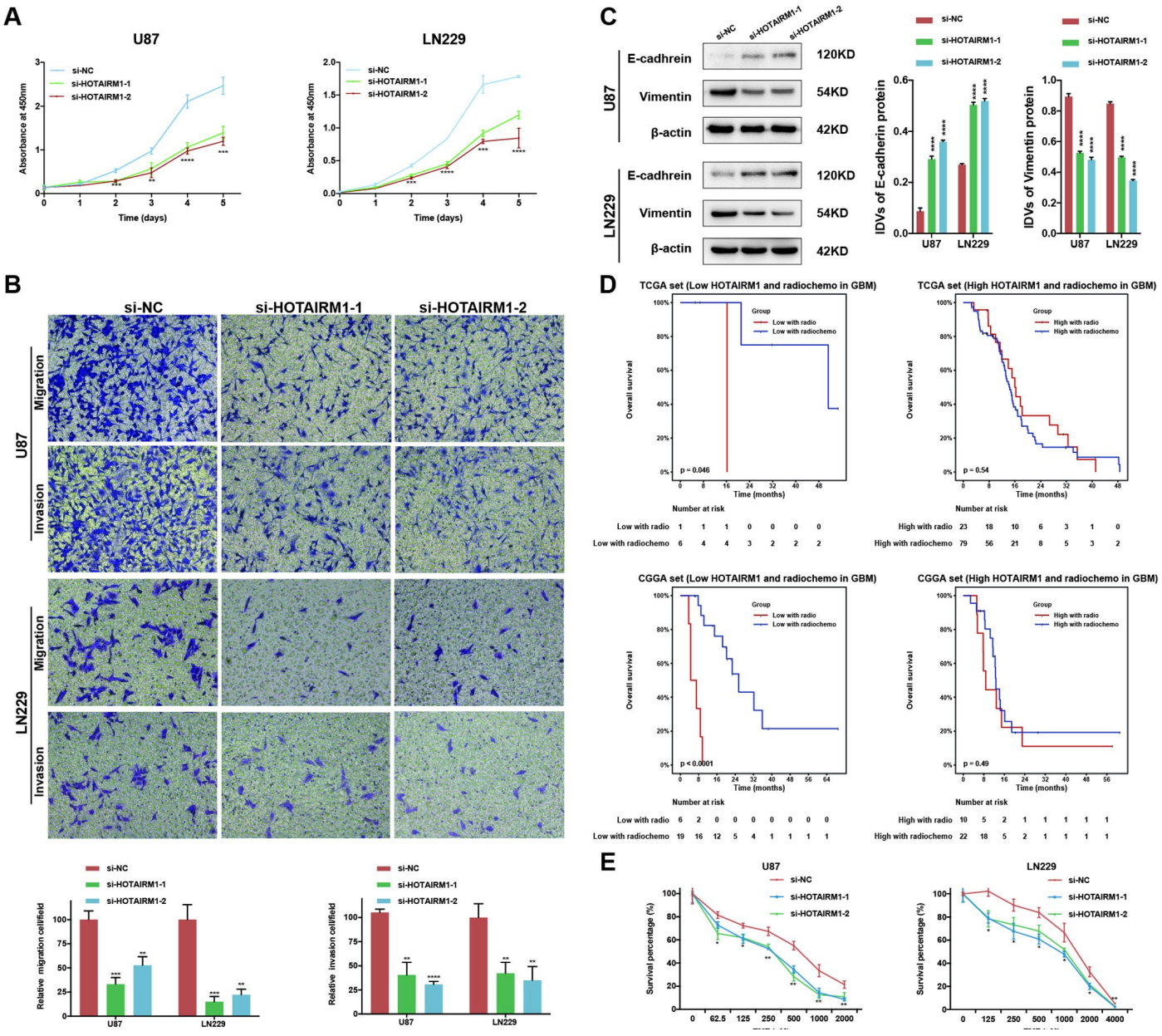

Figure 5. HOTAIRM1 silencing inhibits glioma cell proliferation, migration, invasion, and EMT and increases sensitivity to TMZ in vitro. (**A**) Cell proliferation after transfection of cells with si-HOTAIRM1-1 and -2, as determined with the CCK-8 assay. (**B**) Migration and invasion in U87 and LN229 cells evaluated with transwell assays. (**C**) Western blot analysis of E-cadherin (epithelial marker) and vimentin (mesenchymal marker) expression following HOTAIRM1 knockdown; β-actin served as a loading control. (**D**) Prognostic value of radiochemotherapy compared with radiotherapy alone in high- and low-exp groups. (**E**) Viability of U87 and LN229 cells transfected with siRNA against HOTAIRM1 (si-HOTAIRM1) or negative control siRNA (si-NC) following TMZ treatment at indicated doses. Values represent mean ± SD (n = 3 biological replicates). *P < 0.05, **P < 0.01, ***P < 0.001, ****P < 0.0001 (Student's t test).

that the pattern of immune responses varied according to HOTAIRM1 expression level, which was confirmed by GSEA (Figure 8A–8F and Supplementary Figure 8). An analysis of inflammatory response [21, 22] according to the expression level of HOTAIRM1 revealed that most inflammation-related genes were positively associated with HOTAIRM1 expression except for immunoglobulin G, which was related to B lymphocyte activity (Figure 8G, 8H and Supplementary Figure 9). We then compared the expression levels of six inflammation-related genes including interleukin 1 beta, prostaglandin-endoperoxide synthase 2 (also known as cyclooxygenase 2b), transforming growth factor beta 1, C-C motif chemokine ligand 2, interleukin 6, and signal transducer and activator of transcription 3 [23, 24] between high- and low-exp groups in TCGA and CGGA. All six of these genes were more highly expressed in the high-exp group than in the low-exp group, which was confirmed by quantitative real-time polymerase chain reaction (qRT-PCR) in an independent glioma cohort (Figure 8I–8K). Thus, aberrant HOTAIRM1 expression is associated with a distinct immune and inflammatory phenotype in glioma.

To evaluate the impact of HOTAIRM1 on the tumor microenvironment (TME), we calculated immune and stromal scores and tumor purity in glioma specimens of TCGA and CGGA datasets. HOTAIRM1 expression was positively associated with immune and stromal scores and negatively associated with tumor purity. To determine which type of non-tumor cell contributes to the altered TME, we used gene set variation analysis (GSVA) to estimate the gene set of immune cells and evaluate the correlation between immune cell types and HOTAIRM1 expression. We used a threshold of absolute correlation coefficient > 0.2 and false discovery rate < 0.01 in the two datasets. The results showed that delta T cells, cluster of differentiation 8+ T cells, activated dendritic cells, and regulatory T cells (Tregs) were positively correlated, whereas follicular B helper T cells were negatively correlated with HOTAIRM1 expression (Supplementary Figure 10).

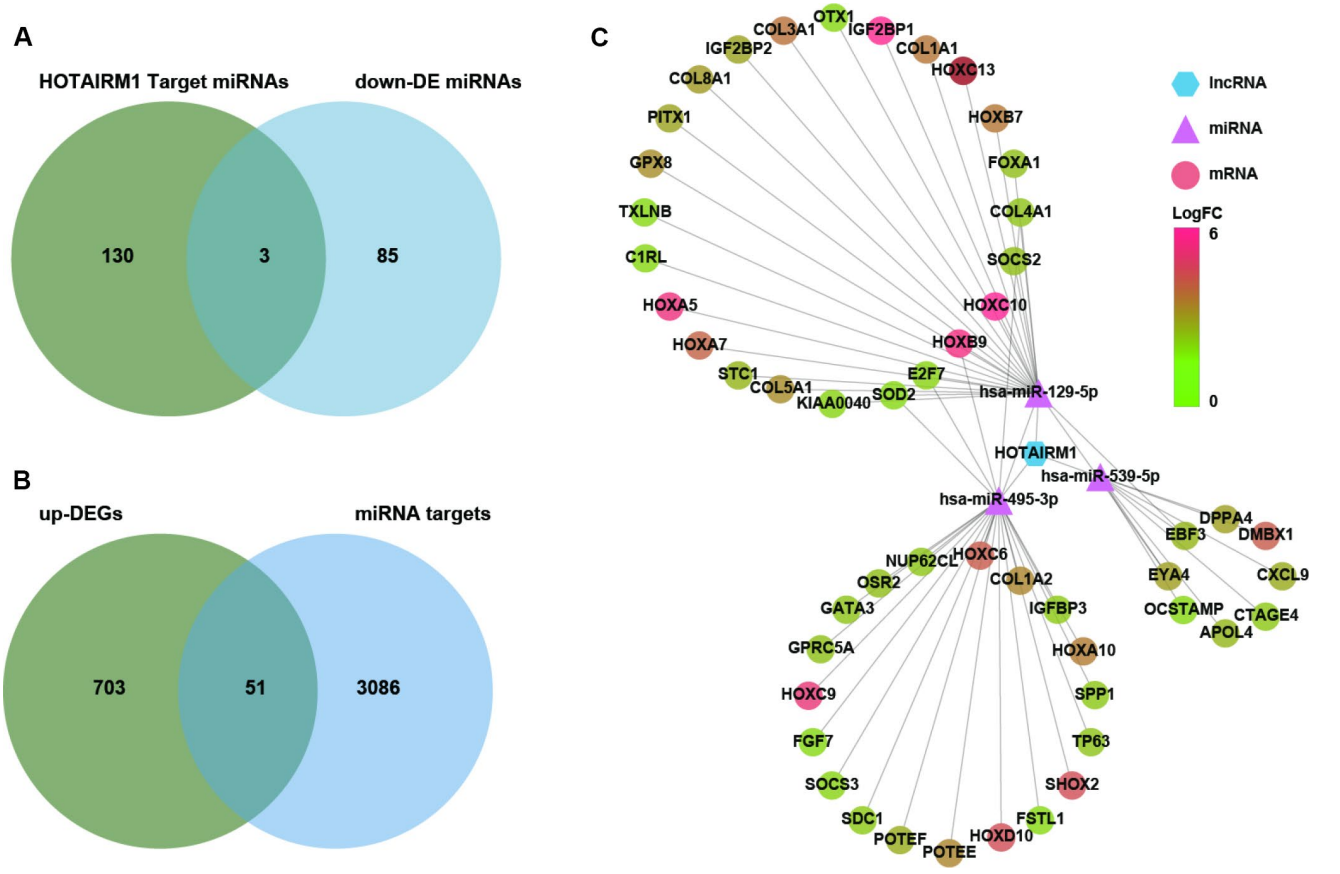

Figure 6. Construction of a HOTAIRM1–miRNA–mRNA network. (**A**) Venn diagram showing the intersection between HOTAIRM1 target miRNAs predicted with DIANA tools and LncBase Predicted v.2 and miRNAs that are differentially downregulated in GBM compared with normal brain tissue ($P < 0.01$). (**B**) Venn diagram showing the intersection between up-DEGs in the high-exp group compared with the low-exp group (log2 fold change > 2; $P < 0.05$) and predicted targets of three miRNAs (hsa-miR-129-5p, hsa-miR-495-3p, and hsa-miR-539-5p). (**C**) Network comprising HOTAIRM1, three miRNAs, and 51 genes generated with Cytoscape v.3.6.1. DE, differential expression.

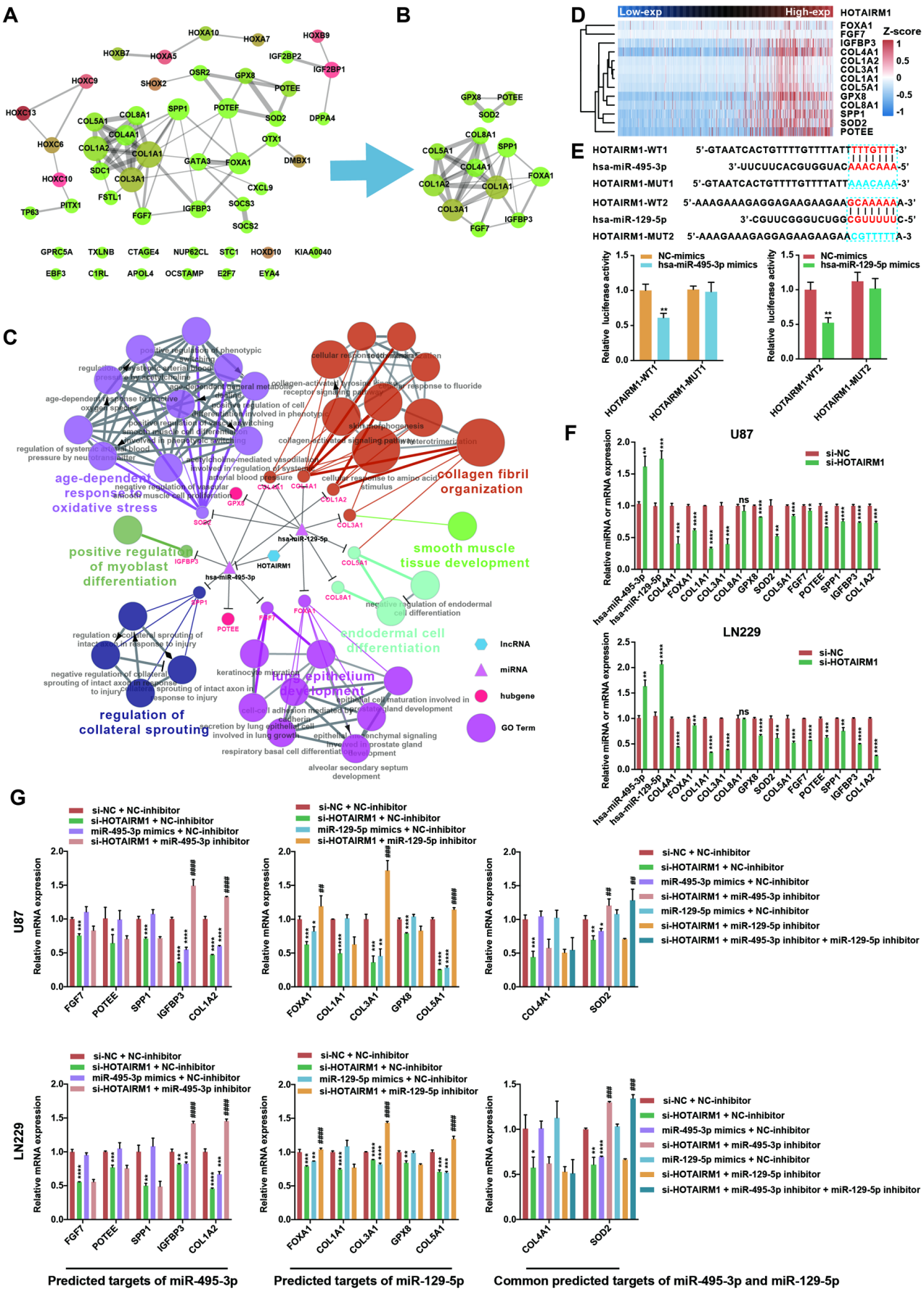
A
B
C
D
E
F
G
HOTAIRM1
Low-exp
High-exp
Z-score
NC-mimics
hsa-miR-495-3p mimics
hsa-miR-129-5p mimics
HOTAIRM1-WT1
HOTAIRM1-MUT1
HOTAIRM1-WT2
HOTAIRM1-MUT2
U87
LN229
si-NC
si-HOTAIRM1
Relative miRNA or mRNA expression
Relative luciferase activity
lncRNA
miRNA
hubgene
GO Term
age-dependent response to oxidative stress
collagen fibril organization
positive regulation of myoblast differentiation
smooth muscle tissue development
endodermal cell differentiation
epithelium development
regulation of collateral sprouting
si-NC + NC-inhibitor
si-HOTAIRM1 + NC-inhibitor
miR-495-3p mimics + NC-inhibitor
si-HOTAIRM1 + miR-495-3p inhibitor
miR-129-5p mimics + NC-inhibitor
si-HOTAIRM1 + miR-129-5p inhibitor
si-HOTAIRM1 + miR-495-3p inhibitor + miR-129-5p inhibitor
Predicted targets of miR-495-3p
Predicted targets of miR-129-5p
Common predicted targets of miR-495-3p and miR-129-5p

Figure 7. Construction of a HOTAIRM1–miRNA–hub gene network. (**A**) PPI network of 51 target genes that are closely related to HOTAIRM1 level generated using the PPI function in Cytoscape v.3.6.1. Node size increased according to the number of neighbors of each gene, and edge size changed from fine to coarse based on the combined score of two adjacent genes. (**B**) Subnetwork consisting of 13 hub genes extracted from (**A**) generated by MCODE in Cytoscape v.3.6.1. (**C**) Network consisting of HOTAIRM1, two miRNAs (hsa-miR-129-5p and hsa-miR-495-3p), and 13 hub genes generated with Cytoscape v.3.6.1. GO analyses of 13 hub genes was performed using ClueGO. (**D**) Expression profile of 13 hub genes in order of increasing HOTAIRM1 expression level in TCGA dataset. (**E**) Schematic representation of putative binding sites of miR-495-3p and miR-129-5p in HOTAIRM1. Relative luciferase activity was determined for HEK-293T cells co-transfected with wild-type HOTAIRM1 overexpression plasmid (HOTAIRM1-WT1) and miR-459-3p mimic or with HOTAIRM1-WT2 and miR-129-5p mimic. **P < 0.01 vs. HOTAIRM1-WT1 + negative control (NC) mimic or HOTAIRM1-WT2 + NC mimic group. (**F**) qRT-PCR analysis of expression levels of miR-129-5p, miR-495-3p, and 13 hub genes after HOTAIRM1 knockdown. ns, no significant difference; *P < 0.05, **P < 0.01, ***P < 0.001, ****P < 0.0001 vs. negative control siRNA (si-NC) group. (**G**) qRT-PCR analysis of the levels of indicated hub genes in U87 and LN229 cells after HOTAIRM1 knockdown and transfection of indicated miRNA inhibitor or mimic. *P < 0.05, **P < 0.01, ***P < 0.001, ****P < 0.0001 vs. si-NC + NC inhibitor group; ##P < 0.01, ###P < 0.001, ####P < 0.0001 vs. si-HOTAIRM1 + NC inhibitor group.

DISCUSSION

LncRNAs are implicated in tumorigenesis and immune system regulation [25] and modulate various aspects of glioma biology including proliferation, migration, invasion, and drug resistance [7, 26]. In this study we found a close association between HOTAIRM1 expression and the clinical and molecular characteristics of glioma. Elevated HOTAIRM1 was linked to high risk factors including older age (≥ 50 years), lower KPS, mesenchymal subtype, wild-type IDH, unmethylated MGMT promoter, and 1p/19q non-codeletion, whereas protective factors such as wild-type PTEN and TP53 were associated with glioma samples showing low HOTAIRM1 expression. These findings indicate that HOTAIRM1 has an oncogenic function in human glioma.

HOTAIRM1 has been shown to function as both an oncogene and tumor suppressor in various solid tumors. For instance, HOTAIRM1 inhibits tumorigenesis by forming ceRNA networks in colorectal cancer, head and neck tumors, gastric cancer, and hepatocellular carcinoma [10–12, 27]. Conversely, HOTAIRM1 promotes breast cancer, lung cancer, and pancreatic ductal adenocarcinoma by directly regulating HOXA1 expression [13, 14, 28, 29]. As a fetal lncRNA [30], HOTAIRM1 is upregulated in glioma [31, 32]. However, the prognostic value of HOTAIRM1 in glioma remains unknown. To address this point, we analyzed TCGA and CGGA cohorts and found that HOTAIRM1 upregulation was independently associated with poor prognosis in glioma patients. Functional analyses revealed that HOTAIRM1 is involved in various malignant behaviors, which is consistent with a recent report [33]. Thus, HOTAIRM1 is an onco-lncRNA in glioma.

Resistance to alkylating agents is the main reason for the poor prognosis of glioma even after chemotherapy. EMT is a key driver of chemotherapy resistance, which is regulated by various lncRNAs. In glioma, HOXA transcript at the distal tip induces the expression of zinc finger E-box-binding homeobox 1 and promotes EMT by sponging miR-101 under hypoxic conditions [34]. In the present study, HOTAIRM1 knockdown inhibited EMT in glioma by reducing the levels of mesenchymal cell markers and increasing those of epithelial cell markers. HOTAIRM1 overexpression was associated with limited clinical benefit from TMZ treatment, whereas HOTAIRM1 knockdown decreased the IC50 for TMZ in two glioma cell lines. These results suggest that HOTAIRM1 can serve as a marker for TMZ resistance and that its inhibition is a useful therapeutic strategy for glioma patients.

HOTAIRM1 was shown to promote tumor malignancy by directly regulating HOXA1 expression in lung cancer and glioma [13, 33]. Consistent with these observations, we found that HOTAIRM1 level was positively associated with that of HOXA family genes in TCGA and CGGA datasets (Supplementary Figure 11). CeRNA networks formed in conjunction with miRNAs and target genes are an important mechanism by which lncRNAs regulate tumorigenesis [26]. We established a ceRNA network comprising HOTAIRM1, hsa-miR-129-5p, hsa-miR-495-3p, and 13 hub genes that was validated with the luciferase assay and by qRT-PCR. Previous studies have demonstrated that hsa-miR-129-5p and hsa-miR-495-3p inhibit cell proliferation, migration, invasion, and EMT and increase drug sensitivity [35–37]. Accordingly, most of the identified 13 hub genes were associated with tumor progression and establishment of the TME [17–19, 38–40]. For example, SPP1 (also known as osteopontin) is known to promote glioma progression by regulating GBM-associated macrophage infiltration [17], while IGFBP3 impairs T cell accumulation in breast cancer [41]. However, hsa-miR-129-5p and hsa-miR-495-3p inhibitors restored the expression of only a subset of hub genes following depletion of HOTAIRM1, indicating that the latter promotes malignancy and regulates the TME in glioma not only by sponging hsa-miR-129-5p and hsa-miR-495-3p but also by enhancing the expression of some hub genes within a non-ceRNA.

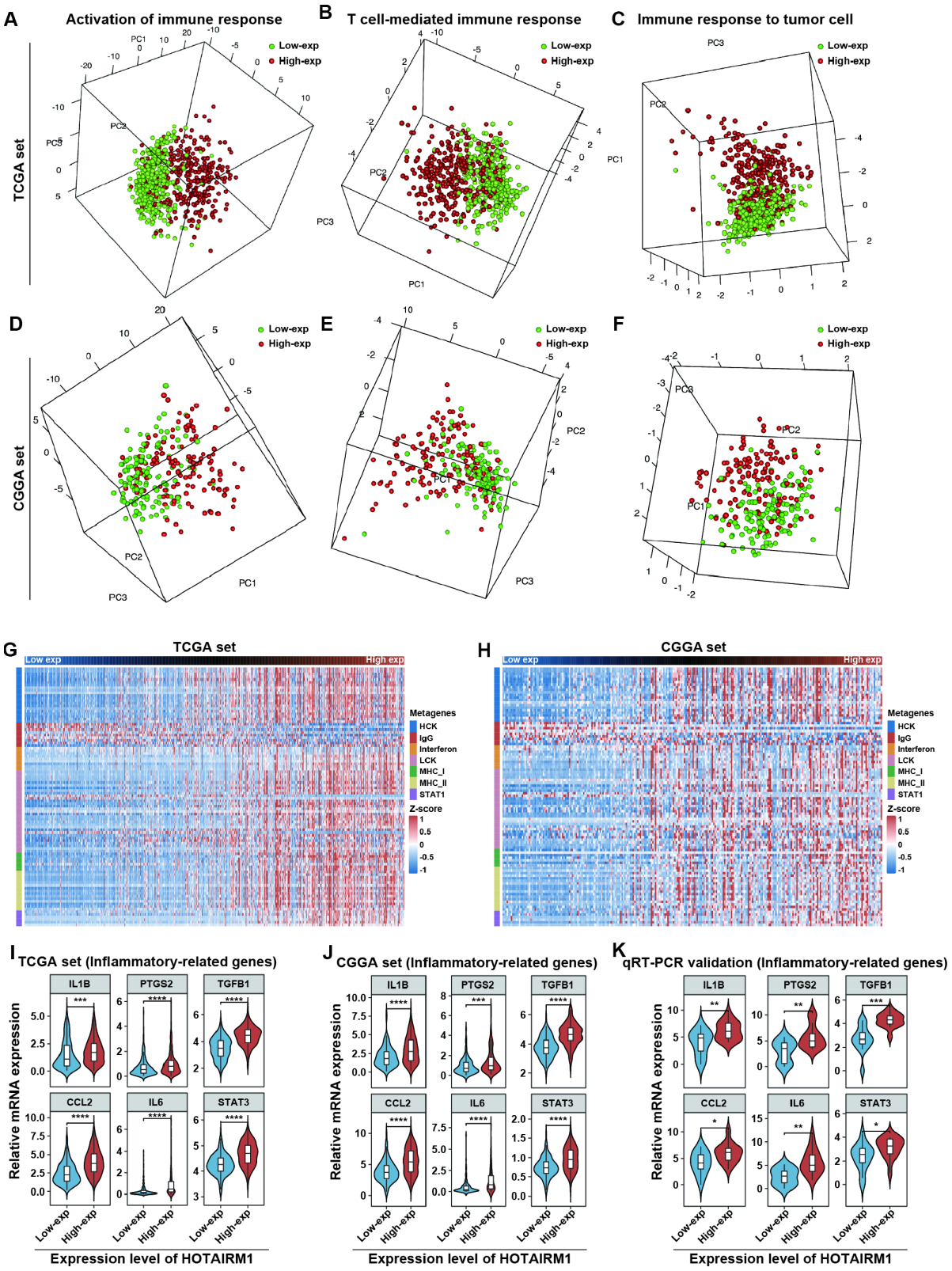

Figure 8. Elevated HOTAIRM1 expression is associated with distinct immune and inflammatory phenotypes. (**A**–**F**) Activation of T cell-mediated immune response and immune response to tumor cells is associated with HOTAIRM1 expression levels in TCGA (**A**–**C**) and CGGA (**D**–**F**). (**G**, **H**) Effect of HOTAIRM1 on inflammation in TCGA (**G**) and CGGA (**H**); gene expression level was normalized to z score. (**I**–**K**) Expression of six inflammation-related genes in TCGA (**I**), CGGA (**J**), and independent glioma samples (**K**) in relation to HOTAIRM1 level. *P < 0.05, **P < 0.01, ***P < 0.001, ****P < 0.0001 vs. low-exp group (Student's t test).

We previously showed that different histological and molecular subtypes of glioma are characterized by distinct local immune status [15, 42]. There is accumulating evidence that lncRNAs regulate immune processes. For example, lincRNA-Cox2 and lincRNA-NeST are regulators of innate immunity [43, 44], and lnc-EGFR mediates immunosuppression in hepatocellular carcinoma by stimulating Treg differentiation [45]. Similarly, HOTAIRM1 was shown to promote an immunosuppressive state in the TME [13]. Here we showed that HOTAIRM1 expression was associated with activation of a T cell-mediated immune response and increased inflammation. HOTAIRM1 also enhanced the immunosuppressive microenvironment of glioma by recruiting Tregs and dendritic cells. Given that EMT is closely related to an immunosuppressive status [46], we speculate that HOTAIRM1 promotes EMT to reprogram immune and inflammatory responses within the glioma microenvironment.

The results of this study demonstrate that HOTAIRM1 can serve as an independent factor for predicting glioma patient survival and response to TMZ chemotherapy. A ceRNA network was established that explains the potential mechanism of action of HOTAIRM1. However, one limitation of the present study is that some of our conclusions were based on the result of a retrospective analysis of publicly available datasets. Thus, additional experiments are needed to clarify the biological function and molecular mechanisms of HOTAIRM1 in glioma.

MATERIALS AND METHODS

Patient samples

Glioma tissue samples (n = 28) for qRT-PCR were collected at the First Hospital of China Medical University. The histological diagnoses of the samples were independently verified by two experienced neuropathologists based on 2010 WHO classification guidelines. Four non-neoplastic brain tissue specimens from cranial injury internal decompression patients served as the negative control. The present study was approved by the Ethics Committee of the First Hospital of China Medical University.

Glioma databases

RNA-seq data, including lncRNA expression in 672 glioma samples were acquired from TCGA database (http://cancergenome.nih.gov/). CGGA transcriptome sequencing data of 274 glioma samples were downloaded from the public database (http://www.cgga.org.cn). After obtaining the RNA-seq data, we annotated each of the samples according to their barcode ID based on available clinical information from University of California, Santa Cruz Xena (https://xenabrowser.net/datapages/) and CGGA databases. A total of 946 glioma samples from TCGA and CGGA with detailed clinical and molecular information were ultimately included in the analysis (Supplementary Table 1). miRNA expression data were downloaded from TCGA database.

Cell lines

U87, LN229, U373, U251, and T98G human glioma cell lines and normal human astrocytes were purchased from American Type Culture Collection (Manassas, VA, USA) and cultured in Dulbecco's Modified Eagle's Medium (DMEM; HyClone, Logan, UT, USA) supplemented with fetal bovine serum (FBS) and penicillin/streptomycin (100 U/ml). DGCs were derived from freshly resected GBM patient specimens and cultured in Roswell Park Memorial Institute 1640 Medium Modified (HyClone) supplemented with FBS and penicillin/streptomycin (100 U/ml). Cells were cultured in an atmosphere of 5% CO_2 at 37°C. All tumor samples were obtained according to the protocol approved by the Ethics Committee of the First Hospital of China Medical University.

Cell transfection

siRNAs for HOTAIRM1 knockdown were synthesized by Sangon Biotech (Shanghai, China) and had the following sequences: si-HOTAIRM1-1 sense, 5′-AGAAACUCCG UGUUACUCATT-3′; si-HOTAIRM1-2 sense, 5′-GAU UAAUCAACCACACUGATT-3'; and si-HOTAIRM1-3 sense, 5′-CCAAUUUAAAUCUAUGGCUTT-3′. hsa-miR-495-3p and hsa-miR-129-5p mimic and inhibitor and a negative control (Sangon Biotech) were used in this study.

qRT-PCR

Total RNA was extracted from samples using TRIzol reagent (Life Technologies, Carlsbad, CA, USA), and cDNA was synthesized using an RNA PCR kit (Takara Bio, Otsu, Japan). qRT-PCR was performed using TB Green Premix Ex Taq II (Tli RNaseH Plus) (Takara Bio), according to the manufacturer's protocol, with the 18S gene sequence serving as the internal standard. To evaluate miR-129-5p and miR-495-3p levels, cDNA was generated with the Taqman miRNA Reverse Transcription kit (Applied Biosystems, Foster City, CA, USA) and qRT-PCR was performed with a TaqMan miRNA assay using TaqMan Universal Master Mix II (Applied Biosystems); the U6 gene served as an endogenous control. qRT-PCR was performed on a LightCycler 96 System (Roche Diagnostics, Basel, Switzerland). All reactions were performed in triplicate. Relative expression levels were calculated with the

$2^{-\Delta\Delta Ct}$ method. The primer sequences and miRNA assay IDs are shown in Supplementary Table 2.

Protein isolation and western blotting

Cells were collected, washed twice with phosphate-buffered saline, and incubated on ice for 20–30 min in radioimmunoprecipitation assay lysis buffer containing 1% benzene sulfonyl fluoride (Beyotime Institute of Biotechnology, Shanghai, China). Protein concentration was measured using a bicinchoninic acid protein assay kit (Beyotime Institute of Biotechnology), and proteins were separated by 6%–15% sodium dodecyl sulfate polyacrylamide gel electrophoresis (Beyotime Institute of Biotechnology), transferred to a polyvinylidene difluoride membrane (Millipore, Billerica, CA, USA), and incubated for 60 min in 5% non-fat milk followed by primary antibodies against E-cadherin (1:10,000; Abcam, Cambridge, UK) and vimentin (1:5000; Abcam). An antibody against β-actin (1:1000; Proteintech, Rosemont, IL, USA) was used as the loading control. The membrane was incubated for 2 h at room temperature with horseradish peroxidase-conjugated secondary antibodies and protein bands were detected by enhanced chemiluminescence. Relative density values were calculated using ImageJ software (National Institutes of Health, Bethesda, MD, USA).

Cell proliferation, wound healing, migration, and invasion assays

Cell proliferation was assessed using CCK-8 (KeyGen Biotech, Nanjing, China). After transfection of HOTAIRM1 siRNA or a negative control siRNA for 48 h, 2×10^3 cells per well were seeded in 96-well plates and cultured for 0, 1, 2, 3, 4, and 5 days. A 10-μl volume of CCK-8 solution was added to each well and incubated at 37°C for 1 h, and the absorbance at 450 nm was measured. All experiments were performed in triplicate.

For the wound healing assay, approximately 1×10^6 cells per cell were seeded in 6-well plates and incubated at 37°C until they reached at least 90% confluence. Wounds were created by scratching cell monolayers with a 1000-μl plastic pipette tip, followed by incubation in fresh medium without serum for 24 h. The initial gap length (0 h) and gap length after 24 h were measured from photomicrographs.

Cell migration and invasion assays were performed using 24-well Transwell chambers with 8-μm pore size polycarbonate membranes (Corning Inc., Corning, NY, USA). For the cell migration assay, 2×10^4 cells were seeded on the top side of the membrane without Matrigel (BD Biosciences, Franklin Lakes, NJ, USA) in serum-free DMEM. The lower chamber was filled with 600 μl DMEM containing 20% FBS. After incubation at 37°C for 20 h, cells migrating to the lower surface of the membrane were fixed and stained with 0.5% crystal violet. For the invasion assay, 6×10^4 cells were seeded on the top side of the membrane pre-coated with Matrigel, and invaded cells on the lower membrane surface were fixed and stained after 24 h. Migration and invasion were quantified by counting cells in three random fields of view per well under 10× objective.

***In vitro* chemosensitivity assay**

TMZ was supplied by Tasly Pharmaceutical (Tianjin, China) and dissolved in dimethyl sulfoxide to a concentration of 100 mM and diluted in cell culture medium to the appropriate final concentration. Approximately 5×10^3 cells per well were seeded in a 96-well plate and incubated at 37°C for 24 h. TMZ was added at concentrations ranging from 62.5 to 4000 μM. Cell viability was assessed with the CCK-8 kit. A dose–response curve was plotted, and IC_{50} values were calculated by non-linear regression (curve fit) with Prism v.7.0a software (GraphPad, La Jolla, CA, USA). Three independent experiments were performed.

Construction of lncRNA–miRNA–mRNA network

miRNAs that were predicted to bind HOTAIRM1 were identified from DIANA tools and LncBase Predicted v.2 (http://www.microrna.gr/LncBase/). LncRNA–miRNA pairs were determined from the intersection of miRNAs that were predicted to bind HOTAIRM1 and those that were downregulated in GBM compared with normal brain tissue ($P < 0.01$). Target genes of overlapping miRNAs were predicted with starBase v.3.0 (http://starbase.sysu.edu.cn), which includes seven prediction algorithms (PITA, RNA22, miRmap, microT, miRanda, PicTar, and TargetScan). miRNA–mRNA pairs were identified by overlapping target genes predicted by at least three algorithms with up-DEGs in the high- vs. low-exp group. lncRNA–miRNA and miRNA–mRNA pairs were used to construct a lncRNA–miRNA–mRNA network using Cytoscape v.3.6.1 software.

Dual luciferase reporter assay

The pmirGLO luciferase vector with putative hsa-miR-495-3p and hsa-miR-129-5p binding sites in HOTAIRM1 and their mutated forms were purchased from Promega (Madison, WI, USA). The plasmid and miRNA mimic were co-transfected into HEK-293T cells, which were lysed 48 h later and tested for firefly and Renilla luciferase activities using the Dual-Luciferase Reporter Assay System (Promega). Renilla luciferase activity served as an internal control.

Bioinformatic analysis

PCA was performed using R package to evaluate genomic expression patterns in relation to HOTAIRM1 expression levels. GO analysis was performed using DAVID (http://david.abcc.ncifcrf.gov/home.jsp) or ClueGO, a Cytoscape plug. Immune score, stromal score, and glioma purity were calculated with the Estimation of Stromal and Immune Cells in Malignant Tumors Using Expression Data R package (https://sourceforge.net/projects/estimateproject/) as previously described [47]. The GSVA package was used to assess the relationship between HOTAIRM1 expression level and immune cell abundance/inflammation in gene sets retrieved from previous studies [21]. GSEA of biological functions was performed (http://software.broadinstitute.org/gsea/index.jsp), and a PPI network was constructed using the STRING protein query function in Cytoscape v.3.6.1. Hub genes in the PPI network were identified with MCODE [48], a Cytoscape v.3.6.1 plug-in.

Statistical analysis

Statistical analyses were performed using Excel 2016 (Microsoft, Redmond, WA, USA), SPSS v.24 (SPSS Inc., Chicago, IL, USA), Prism 7 v.7.0a, or R v.3.5.0 (https://www.r-project.org/) software. Glioma patients were divided into a low- and a high-exp groups according to median expression level of HOTARIM1. Differences in clinical and molecular features between the two groups were evaluated with the Student's t test or χ^2 test, and differences in HOTAIRM1 expression levels between the two groups were evaluated with the Student's t test or by one-way analysis of variance. A Kaplan–Meier survival curve was used to assess the prognostic significance of HOTAIRM1 expression. Uni- and multivariate Cox regression analyses were performed to identify independent prognostic factors for glioma. A two-sided P value < 0.05 was considered statistically significant.

Abbreviations

ATRX: alpha thalassemia/mental retardation syndrome X-linked; CCK-8: Cell Counting Kit-8; ceRNA: competing endogenous RNA; CGGA: Chinese Glioma Genome Atlas; DEG: differentially expressed gene; DGC: differentiated glioblastoma cell; DMEM: Dulbecco's Modified Eagle's Medium; EGFR: epidermal growth factor receptor; EMT: epithelial–mesenchymal transition; FBS: fetal bovine serum; IDH: isocitrate dehydrogenase; GBM: glioblastoma multiforme; GBM-IDHwt: GBM with wild-type IDH; GO: Gene Ontology; GSEA: gene set enrichment analysis; high-exp: high expression of HOTAIRM1; HOTAIRM1: homeobox A transcript antisense RNA myeloid-specific 1; HR: hazard ratio; IGFBP3: insulin-like growth factor-binding protein 3; KPS: Karnofsky performance score; LGG: low-grade glioma; LGG-IDHwt: low-grade glioma with wild-type IDH; lncRNA: long non-coding RNA; low-exp: low expression of HOTAIRM1; MGMT: O-6-methylguanine-DNA methyltransferase; MCODE: Molecular Complex Detection; miRNA: microRNA; OS: overall survival; PCA: principal component analysis; PPI: protein–protein interaction; PTEN: phosphatase and tensin homolog; qRT-PCR: quantitative real-time polymerase chain reaction; siRNA: small interfering RNA; SOD2: superoxide dismutase; SPP1: secreted phosphoprotein 1; TCGA: The Cancer Genome Atlas; TME: tumor microenvironment; TMZ: temozolomide; Treg: regulatory T cell; up-DEG: differentially upregulated gene; WHO: World Health Organization.

AUTHOR CONTRIBUTIONS

QL, WC, and AW designed the study. QL, XL, XX, CP, and CC performed the experiments. QL, GG, and WC performed the bioinformatic and statistical analyses. QL wrote the manuscript. WC and AW revised the manuscript. All authors read and approved the final manuscript.

ACKNOWLEDGMENTS

We thank the members of Dr. AH Wu's laboratory for assistance with this study.

CONFLICTS OF INTEREST

The authors declare that they have no conflict of interests.

FUNDING

This study was supported by the National Natural Science Foundation of China (nos. 81172409, 81472360, and 81872054 to A. Wu; no. 81872057 to P. Cheng; and no. 81502176 to C. Chen); Liaoning Science and Technology Plan Projects (no. 2011225034 to A. Wu); Natural Science Foundation of Liaoning Province (no. 20180550063 to P. Cheng); and National Postdoctoral Program for Innovative Talents (no. BX20180384 to W. Cheng).

REFERENCES

1. Weller M, Wick W, Aldape K, Brada M, Berger M, Pfister SM, Nishikawa R, Rosenthal M, Wen PY, Stupp R, Reifenberger G. Glioma. Nat Rev Dis Primers. 2015; 1:15017. https://doi.org/10.1038/nrdp.2015.17 PMID:27188790

2. Stupp R, Hegi ME, Mason WP, van den Bent MJ, Taphoorn MJ, Janzer RC, Ludwin SK, Allgeier A, Fisher B, Belanger K, Hau P, Brandes AA, Gijtenbeek J, et al, and European Organisation for Research and Treatment of Cancer Brain Tumour and Radiation Oncology Groups, and National Cancer Institute of Canada Clinical Trials Group. Effects of radiotherapy with concomitant and adjuvant temozolomide versus radiotherapy alone on survival in glioblastoma in a randomised phase III study: 5-year analysis of the EORTC-NCIC trial. Lancet Oncol. 2009; 10:459–66. https://doi.org/10.1016/S1470-2045(09)70025-7 PMID:19269895

3. Lim M, Xia Y, Bettegowda C, Weller M. Current state of immunotherapy for glioblastoma. Nat Rev Clin Oncol. 2018; 15:422–42. https://doi.org/10.1038/s41571-018-0003-5 PMID:29643471

4. Barthel FP, Wesseling P, Verhaak RG. Reconstructing the molecular life history of gliomas. Acta Neuropathol. 2018; 135:649–70. https://doi.org/10.1007/s00401-018-1842-y PMID:29616301

5. Derrien T, Johnson R, Bussotti G, Tanzer A, Djebali S, Tilgner H, Guernec G, Martin D, Merkel A, Knowles DG, Lagarde J, Veeravalli L, Ruan X, et al. The GENCODE v7 catalog of human long noncoding RNAs: analysis of their gene structure, evolution, and expression. Genome Res. 2012; 22:1775–89. https://doi.org/10.1101/gr.132159.111 PMID:22955988

6. Zhang JX, Han L, Bao ZS, Wang YY, Chen LY, Yan W, Yu SZ, Pu PY, Liu N, You YP, Jiang T, Kang CS, and Chinese Glioma Cooperative Group. HOTAIR, a cell cycle-associated long noncoding RNA and a strong predictor of survival, is preferentially expressed in classical and mesenchymal glioma. Neuro Oncol. 2013; 15:1595–603. https://doi.org/10.1093/neuonc/not131 PMID:24203894

7. Liu L, Cui S, Wan T, Li X, Tian W, Zhang R, Luo L, Shi Y. Long non-coding RNA HOTAIR acts as a competing endogenous RNA to promote glioma progression by sponging miR-126-5p. J Cell Physiol. 2018; 233:6822–31. https://doi.org/10.1002/jcp.26432 PMID:29319172

8. Fujisaka Y, Iwata T, Tamai K, Nakamura M, Mochizuki M, Shibuya R, Yamaguchi K, Shimosegawa T, Satoh K. Long non-coding RNA HOTAIR up-regulates chemokine (C-C motif) ligand 2 and promotes proliferation of macrophages and myeloid-derived suppressor cells in hepatocellular carcinoma cell lines. Oncol Lett. 2018; 15:509–14. https://doi.org/10.3892/ol.2017.7322 PMID:29387231

9. Wang XQ, Dostie J. Reciprocal regulation of chromatin state and architecture by HOTAIRM1 contributes to temporal collinear HOXA gene activation. Nucleic Acids Res. 2017; 45:1091–104. https://doi.org/10.1093/nar/gkw966 PMID:28180285

10. Wan L, Kong J, Tang J, Wu Y, Xu E, Lai M, Zhang H. HOTAIRM1 as a potential biomarker for diagnosis of colorectal cancer functions the role in the tumour suppressor. J Cell Mol Med. 2016; 20:2036–44. https://doi.org/10.1111/jcmm.12892 PMID:27307307

11. Zheng M, Liu X, Zhou Q, Liu G. HOTAIRM1 competed endogenously with miR-148a to regulate DLGAP1 in head and neck tumor cells. Cancer Med. 2018; 7:3143–56. https://doi.org/10.1002/cam4.1523 PMID:29905017

12. Lu R, Zhao G, Yang Y, Jiang Z, Cai J, Zhang Z, Hu H. Long noncoding RNA HOTAIRM1 inhibits cell progression by regulating miR-17-5p/ PTEN axis in gastric cancer. J Cell Biochem. 2019; 120:4952–65. https://doi.org/10.1002/jcb.27770 PMID:30302796

13. Tian X, Ma J, Wang T, Tian J, Zhang Y, Mao L, Xu H, Wang S. Long Non-Coding RNA HOXA Transcript Antisense RNA Myeloid-Specific 1-HOXA1 Axis Downregulates the Immunosuppressive Activity of Myeloid-Derived Suppressor Cells in Lung Cancer. Front Immunol. 2018; 9:473. https://doi.org/10.3389/fimmu.2018.00473 PMID:29662483

14. Luo Y, He Y, Ye X, Song J, Wang Q, Li Y, Xie X. High Expression of Long Noncoding RNA HOTAIRM1 is Associated with the Proliferation and Migration in Pancreatic Ductal Adenocarcinoma. Pathol Oncol Res. 2019; 15:241–11. https://doi.org/10.1007/s12253-018-00570-4 PMID:30613920

15. Zhang C, Cheng W, Ren X, Wang Z, Liu X, Li G, Han S, Jiang T, Wu A. Tumor Purity as an Underlying Key Factor in Glioma. Clin Cancer Res. 2017; 23:6279–91. https://doi.org/10.1158/1078-0432.CCR-16-2598 PMID:28754819

16. Kopp F, Mendell JT. Functional Classification and Experimental Dissection of Long Noncoding RNAs. Cell. 2018; 172:393–407. https://doi.org/10.1016/j.cell.2018.01.011 PMID:29373828

17. Wei J, Marisetty A, Schrand B, Gabrusiewicz K, Hashimoto Y, Ott M, Grami Z, Kong LY, Ling X, Caruso H, Zhou S, Wang YA, Fuller GN, et al. Osteopontin mediates glioblastoma-associated macrophage infiltration and is a potential therapeutic target. J Clin Invest. 2019; 129:137–49.

https://doi.org/10.1172/JCI121266 PMID:30307407

18. Scully T, Scott CD, Firth SM, Pintar JE, Twigg SM, Baxter RC. Contrasting effects of IGF binding protein-3 expression in mammary tumor cells and the tumor microenvironment. Exp Cell Res. 2019; 374:38–45. https://doi.org/10.1016/j.yexcr.2018.11.006 PMID:30419192

19. Seo YS, Kim HS, Lee AY, Chun JM, Kim SB, Moon BC, Kwon BI. Codonopsis lanceolata attenuates allergic lung inflammation by inhibiting Th2 cell activation and augmenting mitochondrial ROS dismutase (SOD2) expression. Sci Rep. 2019; 9:2312. https://doi.org/10.1038/s41598-019-38782-6 PMID:30783201

20. Yeh CR, Ou ZY, Xiao GQ, Guancial E, Yeh S. Infiltrating T cells promote renal cell carcinoma (RCC) progression via altering the estrogen receptor β-DAB2IP signals. Oncotarget. 2015; 6:44346–59. https://doi.org/10.18632/oncotarget.5884 PMID:26587829

21. Wang Z, Zhang C, Liu X, Wang Z, Sun L, Li G, Liang J, Hu H, Liu Y, Zhang W, Jiang T. Molecular and clinical characterization of PD-L1 expression at transcriptional level via 976 samples of brain glioma. OncoImmunology. 2016; 5:e1196310. https://doi.org/10.1080/2162402X.2016.1196310 PMID:27999734

22. Zou CY, Guan GF, Zhu C, Liu TQ, Guo Q, Cheng W, Wu AH. Costimulatory checkpoint SLAMF8 is an independent prognosis factor in glioma. CNS Neurosci Ther. 2019; 25:333–42. https://doi.org/10.1111/cns.13041 PMID:30105842

23. Mantovani A, Allavena P, Sica A, Balkwill F. Cancer-related inflammation. Nature. 2008; 454:436–44. https://doi.org/10.1038/nature07205 PMID:18650914

24. Diakos CI, Charles KA, McMillan DC, Clarke SJ. Cancer-related inflammation and treatment effectiveness. Lancet Oncol. 2014; 15:e493–503. https://doi.org/10.1016/S1470-2045(14)70263-3 PMID:25281468

25. Huarte M. The emerging role of lncRNAs in cancer. Nat Med. 2015; 21:1253–61. https://doi.org/10.1038/nm.3981 PMID:26540387

26. Yu M, Xue Y, Zheng J, Liu X, Yu H, Liu L, Li Z, Liu Y. Linc00152 promotes malignant progression of glioma stem cells by regulating miR-103a-3p/FEZF1/CDC25A pathway. Mol Cancer. 2017; 16:110. https://doi.org/10.1186/s12943-017-0677-9 PMID:28651608

27. Zhang Y, Mi L, Xuan Y, Gao C, Wang YH, Ming HX, Liu J. LncRNA HOTAIRM1 inhibits the progression of hepatocellular carcinoma by inhibiting the Wnt signaling pathway. Eur Rev Med Pharmacol Sci. 2018; 22:4861–68. PMID:30070317

28. Su X, Malouf GG, Chen Y, Zhang J, Yao H, Valero V, Weinstein JN, Spano JP, Meric-Bernstam F, Khayat D, Esteva FJ. Comprehensive analysis of long non-coding RNAs in human breast cancer clinical subtypes. Oncotarget. 2014; 5:9864–76. https://doi.org/10.18632/oncotarget.2454 PMID:25296969

29. Zhou Y, Gong B, Jiang ZL, Zhong S, Liu XC, Dong K, Wu HS, Yang HJ, Zhu SK. Microarray expression profile analysis of long non-coding RNAs in pancreatic ductal adenocarcinoma. Int J Oncol. 2015; 48:670–80. https://doi.org/10.3892/ijo.2015.3292 PMID:26676849

30. Lin M, Pedrosa E, Shah A, Hrabovsky A, Maqbool S, Zheng D, Lachman HM. RNA-Seq of Human Neurons Derived from iPS Cells Reveals Candidate Long Non-Coding RNAs Involved in Neurogenesis and Neuropsychiatric Disorders. PLoS ONE. 2011; 6:e23356–12. https://doi.org/10.1371/journal.pone.0023356 PMID:21915259

31. Zhang X, Sun S, Pu JK, Tsang AC, Lee D, Man VO, Lui WM, Wong ST, Leung GK. Long non-coding RNA expression profiles predict clinical phenotypes in glioma. Neurobiol Dis. 2012; 48:1–8. https://doi.org/10.1016/j.nbd.2012.06.004 PMID:22709987

32. Chen Y, Wu JJ, Lin XB, Bao Y, Chen ZH, Zhang CR, Cai Z, Zhou JY, Ding MH, Wu XJ, Sun W, Qian J, Zhang L, et al. Differential lncRNA expression profiles in recurrent gliomas compared with primary gliomas identified by microarray analysis. Int J Clin Exp Med. 2015; 8:5033–43. PMID:26131076

33. Li Q, Dong C, Cui J, Wang Y, Hong X. Over-expressed lncRNA HOTAIRM1 promotes tumor growth and invasion through up-regulating HOXA1 and sequestering G9a/EZH2/Dnmts away from the HOXA1 gene in glioblastoma multiforme. J Exp Clin Cancer Res. 2018; 37:1–15. https://doi.org/10.1186/s13046-018-0941-x PMID:30376874

34. Zhang S, Wang W, Liu G, Xie S, Li Q, Li Y, Lin Z. Long non-coding RNA HOTTIP promotes hypoxia-induced epithelial-mesenchymal transition of malignant glioma by regulating the miR-101/ZEB1 axis. Biomed Pharmacother. 2017; 95:711–20. https://doi.org/10.1016/j.biopha.2017.08.133

PMID:28886531

35. Gao Y, Feng B, Han S, Lu L, Chen Y, Chu X, Wang R, Chen L. MicroRNA-129 in Human Cancers: from Tumorigenesis to Clinical Treatment. Cell Physiol Biochem. 2016; 39:2186–202. https://doi.org/10.1159/000447913 PMID:27802440

36. Bai Z, Wang J, Wang T, Li Y, Zhao X, Wu G, Yang Y, Deng W, Zhang Z. The MiR-495/Annexin A3/P53 Axis Inhibits the Invasion and EMT of Colorectal Cancer Cells. Cell Physiol Biochem. 2017; 44:1882–95. https://doi.org/10.1159/000485877 PMID:29224019

37. Guo J, Jin D, Wu Y, Yang L, Du J, Gong K, Chen W, Dai J, Miao S, Xi S. The miR 495-UBE2C-ABCG2/ERCC1 axis reverses cisplatin resistance by downregulating drug resistance genes in cisplatin-resistant non-small cell lung cancer cells. EBioMedicine. 2018; 35:204–21. https://doi.org/10.1016/j.ebiom.2018.08.001 PMID:30146342

38. Huang T, Wang L, Liu D, Li P, Xiong H, Zhuang L, Sun L, Yuan X, Qiu H. FGF7/FGFR2 signal promotes invasion and migration in human gastric cancer through upregulation of thrombospondin-1. Int J Oncol. 2017; 50:1501–12. https://doi.org/10.3892/ijo.2017.3927 PMID:28339036

39. Tong Z, Meng X, Wang J, Wang L. MicroRNA-212 inhibits the proliferation and invasion of human renal cell carcinoma by targeting FOXA1. Mol Med Rep. 2018; 17:1361–67. https://doi.org/10.3892/mmr.2017.7956 PMID:29115609

40. Gao YF, Mao XY, Zhu T, Mao CX, Liu ZX, Wang ZB, Li L, Li X, Yin JY, Zhang W, Zhou HH, Liu ZQ. COL3A1 and SNAP91: novel glioblastoma markers with diagnostic and prognostic value. Oncotarget. 2016; 7:70494–503. https://doi.org/10.18632/oncotarget.12038 PMID:27655637

41. Scully T, Scott CD, Firth SM, Sedger LM, Pintar JE, Twigg SM, Baxter RC. Enhancement of mammary tumour growth by IGFBP-3 involves impaired T cell accumulation. Endocr Relat Cancer. 2018; 25:111–22. https://doi.org/10.1530/ERC-17-0384 PMID:29217518

42. Cheng W, Ren X, Zhang C, Cai J, Liu Y, Han S, Wu A. Bioinformatic profiling identifies an immune-related risk signature for glioblastoma. Neurology. 2016; 86:2226–34. https://doi.org/10.1212/WNL.0000000000002770 PMID:27225222

43. Carpenter S, Aiello D, Atianand MK, Ricci EP, Gandhi P, Hall LL, Byron M, Monks B, Henry-Bezy M, Lawrence JB, O'Neill LA, Moore MJ, Caffrey DR, Fitzgerald KA. A long noncoding RNA mediates both activation and repression of immune response genes. Science. 2013; 341:789–92. https://doi.org/10.1126/science.1240925 PMID:23907535

44. Gomez JA, Wapinski OL, Yang YW, Bureau JF, Gopinath S, Monack DM, Chang HY, Brahic M, Kirkegaard K. The NeST long ncRNA controls microbial susceptibility and epigenetic activation of the interferon-γ locus. Cell. 2013; 152:743–54. https://doi.org/10.1016/j.cell.2013.01.015 PMID:23415224

45. Jiang R, Tang J, Chen Y, Deng L, Ji J, Xie Y, Wang K, Jia W, Chu WM, Sun B. The long noncoding RNA lnc-EGFR stimulates T-regulatory cells differentiation thus promoting hepatocellular carcinoma immune evasion. Nat Commun. 2017; 8:15129. https://doi.org/10.1038/ncomms15129 PMID:28541302

46. Lou Y, Diao L, Cuentas ER, Denning WL, Chen L, Fan YH, Byers LA, Wang J, Papadimitrakopoulou VA, Behrens C, Rodriguez JC, Hwu P, Wistuba II, et al. Epithelial-Mesenchymal Transition Is Associated with a Distinct Tumor Microenvironment Including Elevation of Inflammatory Signals and Multiple Immune Checkpoints in Lung Adenocarcinoma. Clin Cancer Res. 2016; 22:3630–42. https://doi.org/10.1158/1078-0432.CCR-15-1434 PMID:26851185

47. Yoshihara K, Shahmoradgoli M, Martínez E, Vegesna R, Kim H, Torres-Garcia W, Treviño V, Shen H, Laird PW, Levine DA, Carter SL, Getz G, Stemke-Hale K, et al. Inferring tumour purity and stromal and immune cell admixture from expression data. Nat Commun. 2013; 4:1–11. https://doi.org/10.1038/ncomms3612 PMID:24113773

48. Bader GD, Hogue CW. An automated method for finding molecular complexes in large protein interaction networks. BMC Bioinformatics. 2003; 4:2. https://doi.org/10.1186/1471-2105-4-2 PMID:12525261

SUPPLEMENTARY MATERIALS

Supplementary Figures

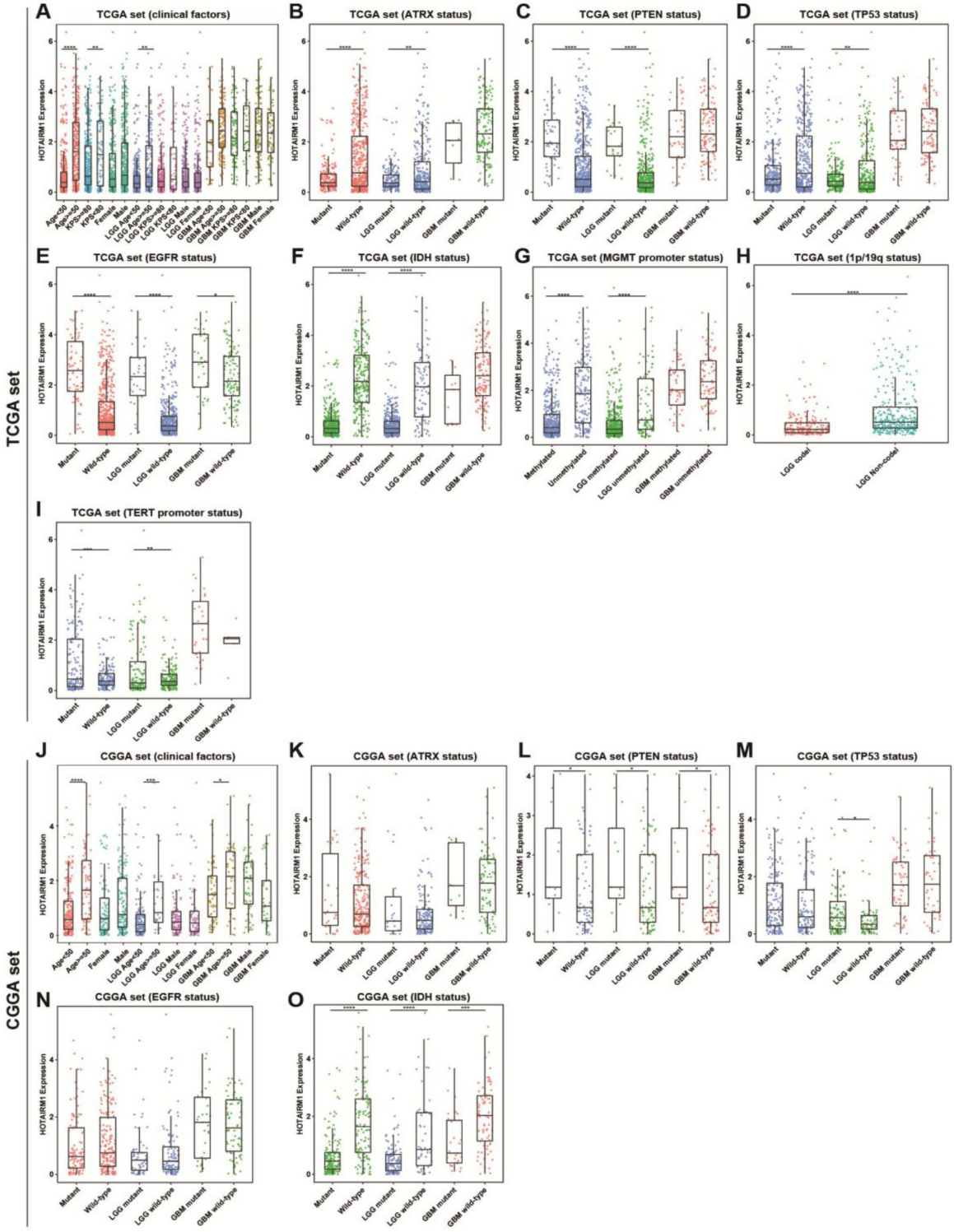

Supplementary Figure 1. Distribution of HOTAIRM1 expression level associated with clinical and molecular features. Distribution of HOTAIRM1 expression level in TCGA (**A**–**I**) and CGGA (**J**–**O**). ns, no significant difference, *p < 0.05, **p < 0.01, ***p < 0.001, ****p < 0.0001, values represented as the mean ± SD, Student's t-test.

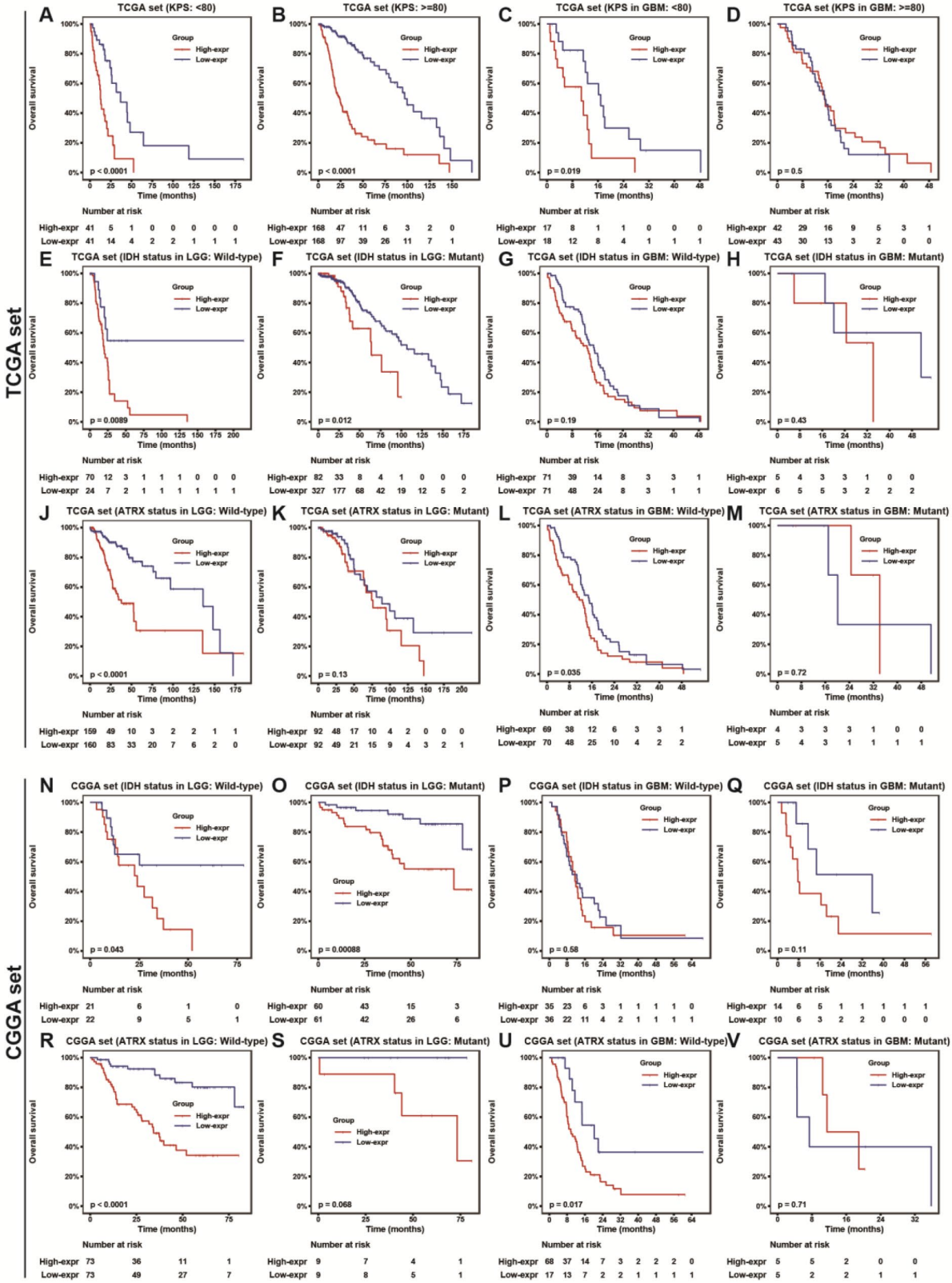

Supplementary Figure 2. Application of HOTAIRM1 in cohorts stratified by clinical and molecular features. (**A**–**D**) Prognostic value of HOTAIRM1 for the KPS in glioma or GBM in TCGA. HOTAIRM1 showed predictive value in LGG cohorts stratified by IDH status in TCGA (**E**, **F**) and CGGA (**N**, **O**) but not in GBM cohorts (**G**, **H**, **P**, **Q**). High HOTAIRM1 expression indicated a poor prognosis in LGG or GBM with ATRX-wt (**J**, **L**, **R**, **U**) but not in LGG or GBM with ATRX-mut (**K**, **M**, **S**, **V**)

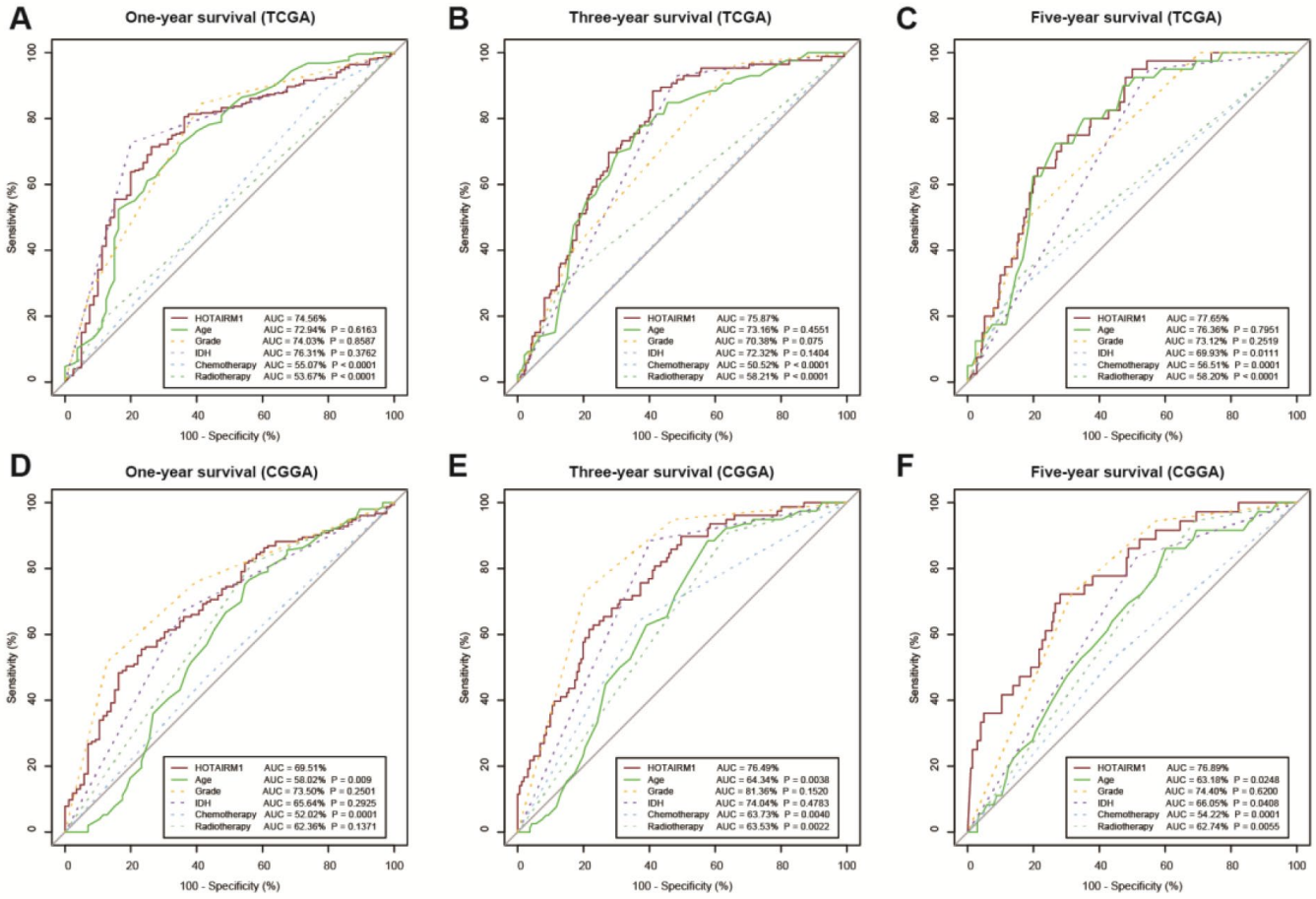

Supplementary Figure 3. HOTAIRM1 as a predictor of survival in glioma patients. HOTAIRM1 expression levels predicted one-year, three-year, and five-year survival in TCGA (**A**–**C**) and CGGA (**D**–**F**).

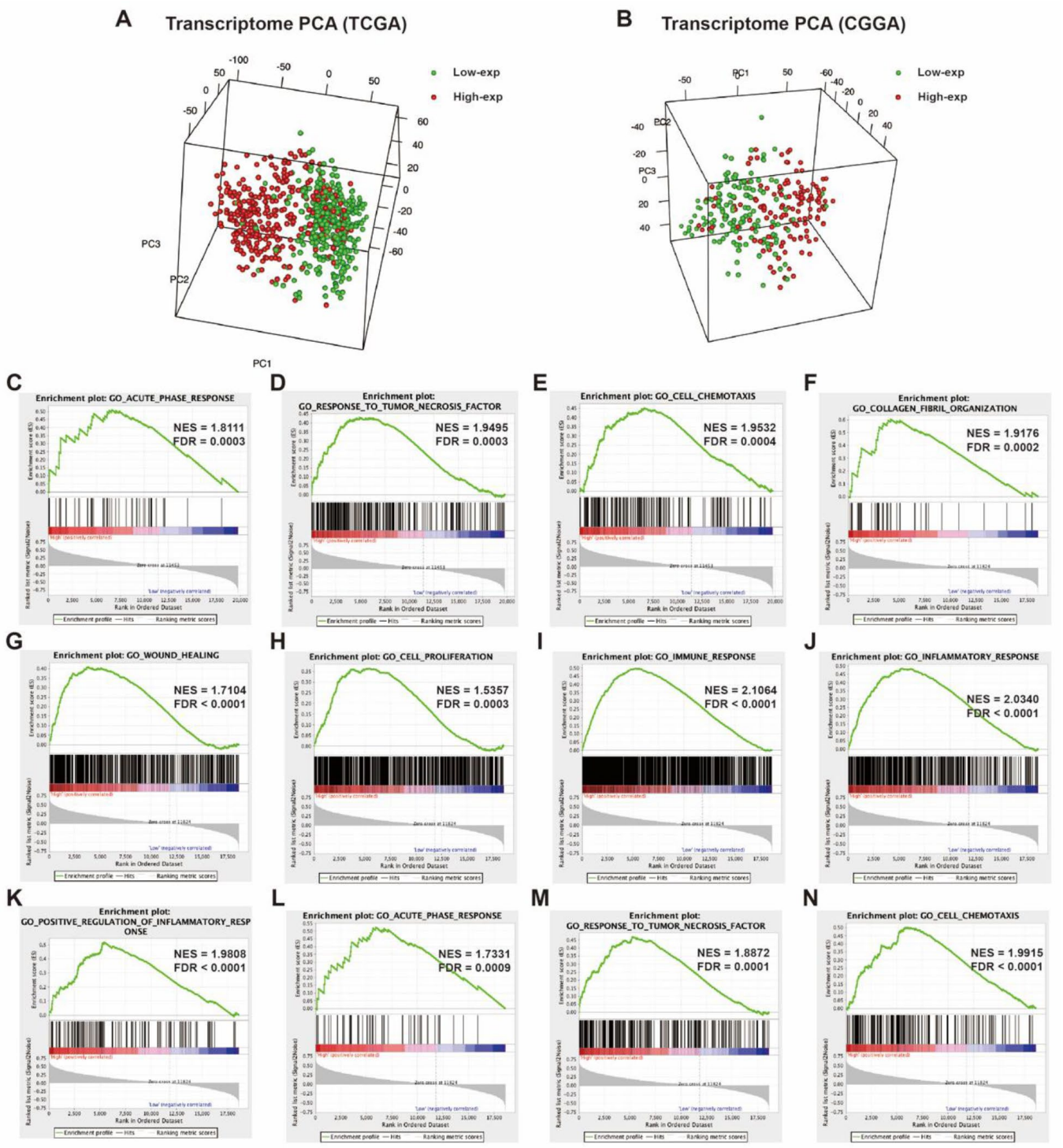

Supplementary Figure 4. Functional analysis of HOTAIRM1 in glioma. HOTAIRM1 was closely correlated with transcriptome expression profiles in TCGA (**A**) and CGGA (**B**). Biologic functions of HOTAIRM1 were confirmed by GSEA in TCGA (**C**-**E**) and CGGA (**F**–**N**). High-exp, high expression of HOTAIRM1; Low-exp, low expression of HOTAIRM1.

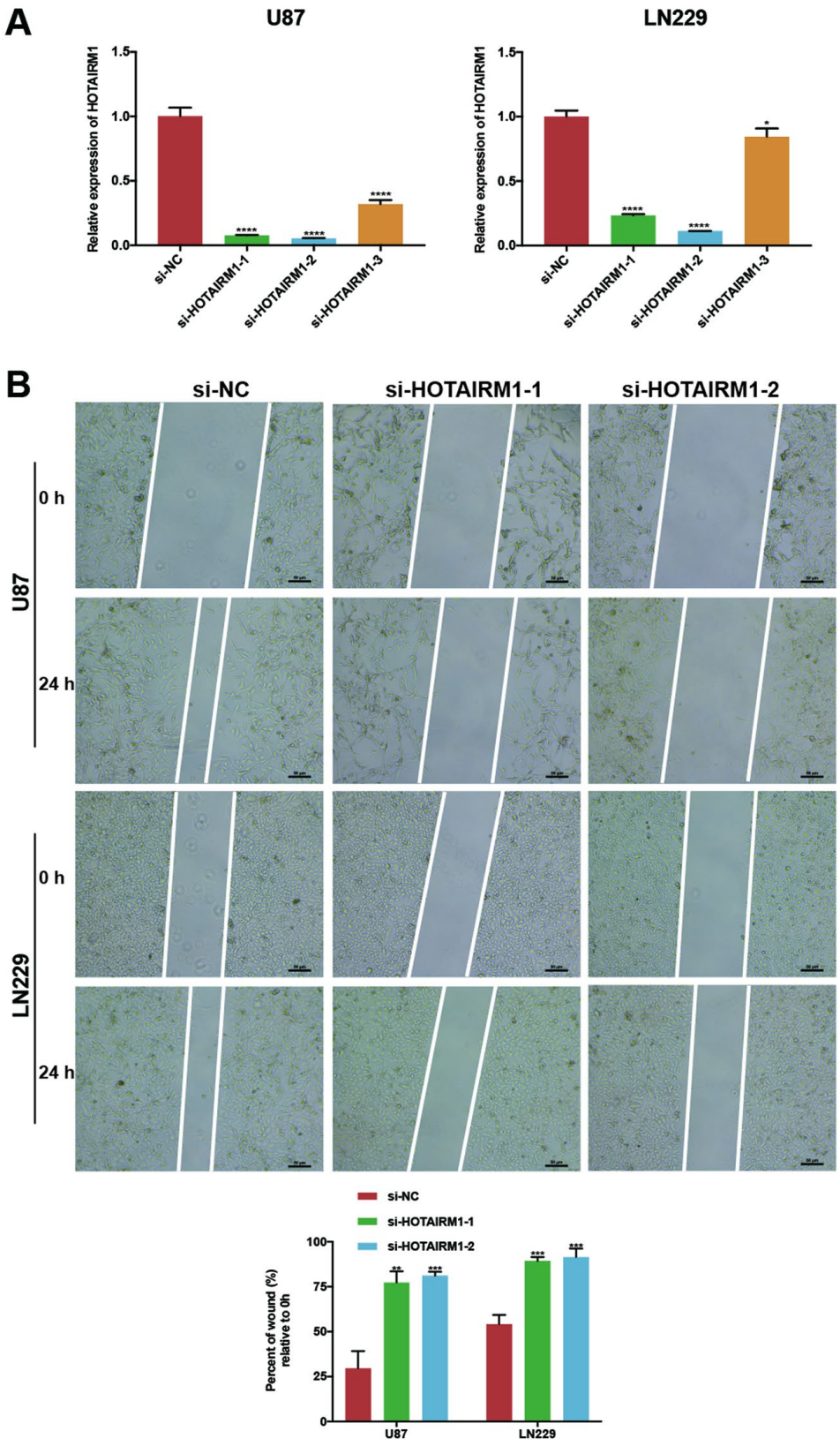

Supplementary Figure 5. HOTAIRM1 promotes cell migration *in vitro*. (**A**) Knockdown efficiency of si-HOTAIRM1-1, -2, and -3 in U87 and LN229 cells assessed by qRT-PCR. (**B**) Wound-healing assays were performed to evaluate the effect of si-HOTAIRM1 on cell migration. *p < 0.05, **p < 0.01, ***p < 0.001, ****p < 0.0001, values represented as the mean ± SD, Student's t-test.

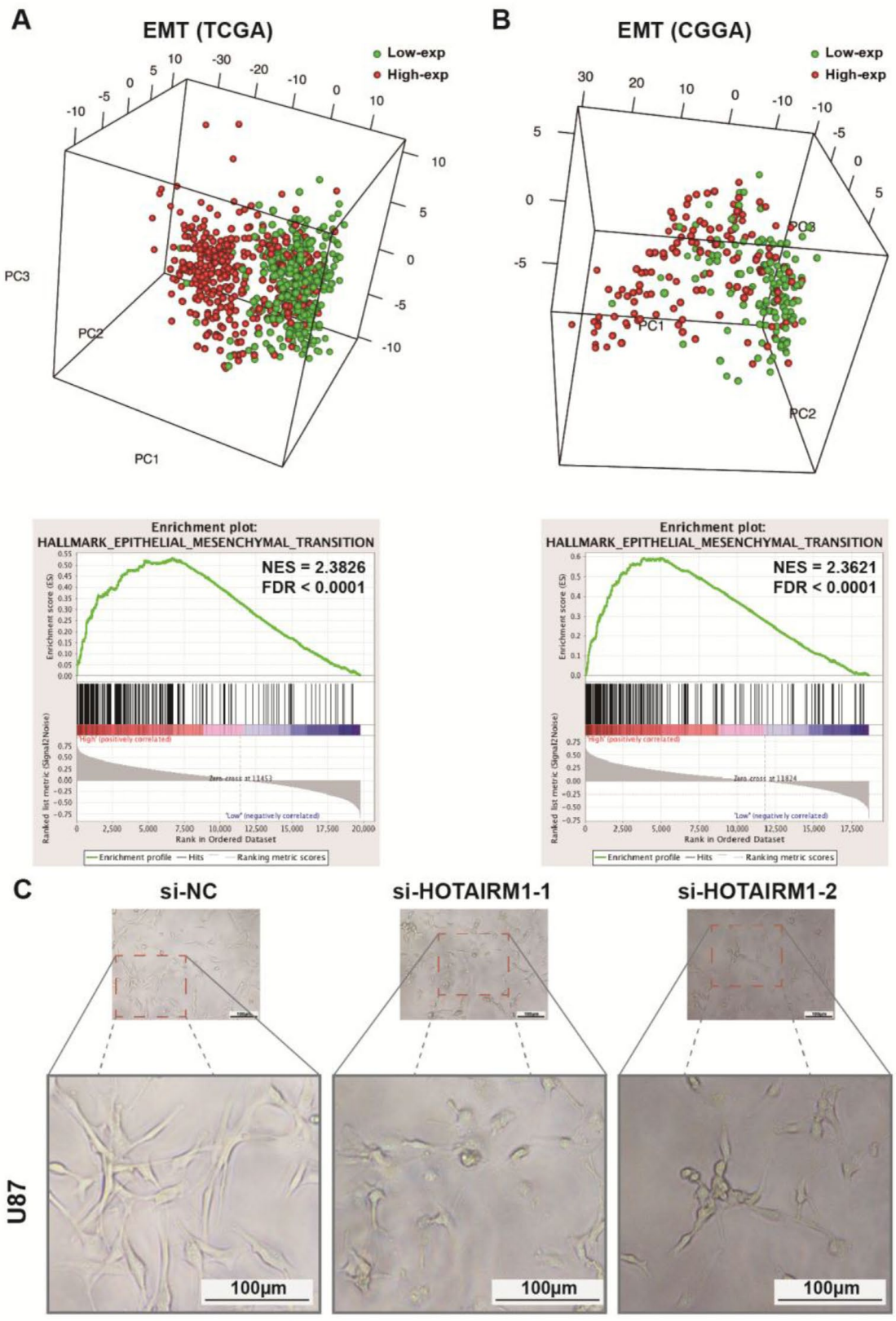

Supplementary Figure 6. HOTAIRM1 was correlated with EMT. (**A**) EMT differed between the high-exp and low-exp groups in TCGA and CGGA. (**B**) GSEA was performed to validate the effect of HOTAIRM1 on EMT in TCGA and CGGA. (**C**) Photomicrograph of U87 ten days after first transfection (×20 magnification; second transfection was performed five days after first transfection to maintain silence efficiency). EMT, epithelial-mesenchymal transition. High-exp, high expression of HOTAIRM1; Low-exp, low expression of HOTAIRM1.

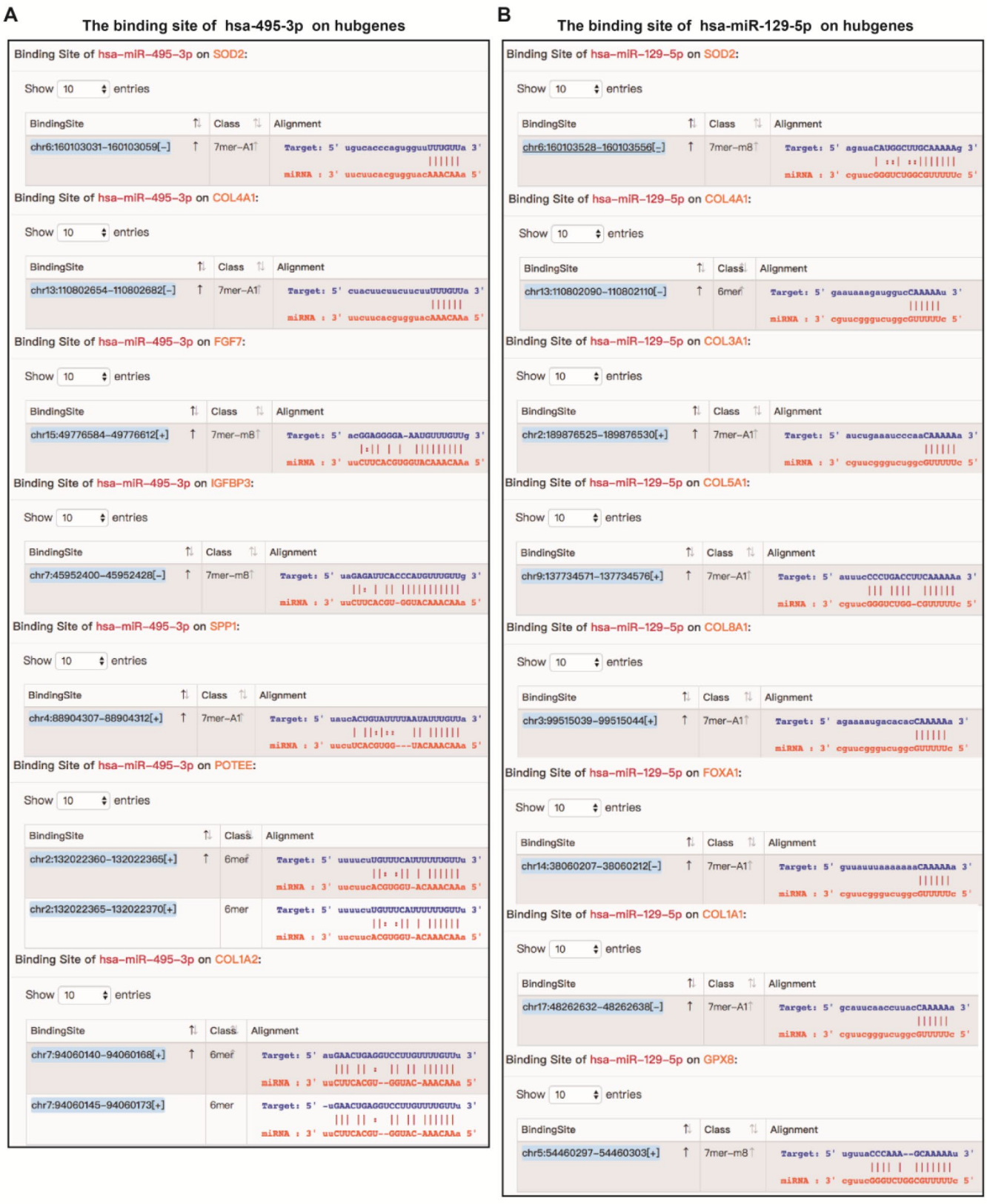

Supplementary Figure 7. The binding site of hsa-miR-495-3p and hsa-miR-129-5p on hub genes predicted with starBase v3.0 (http://starbase.sysu.edu.cn).

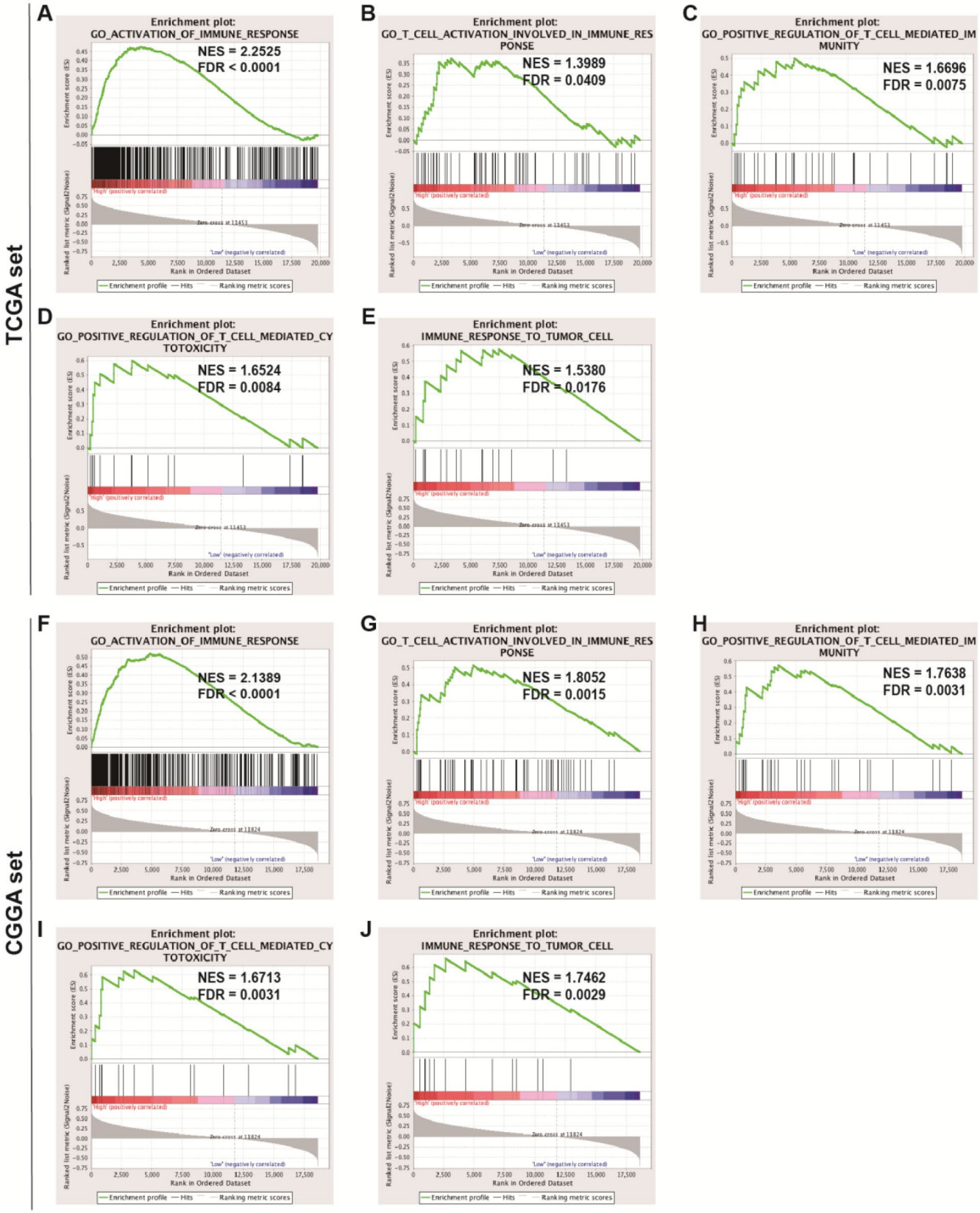

Supplementary Figure 8. Patients with high HOTAIRM1 expression showed a clear immune phenotype. GSEA was performed to confirm the effect of HOTAIRM1 on immune-related gene sets in TCGA (**A**–**E**) and CGGA (**F**–**J**).

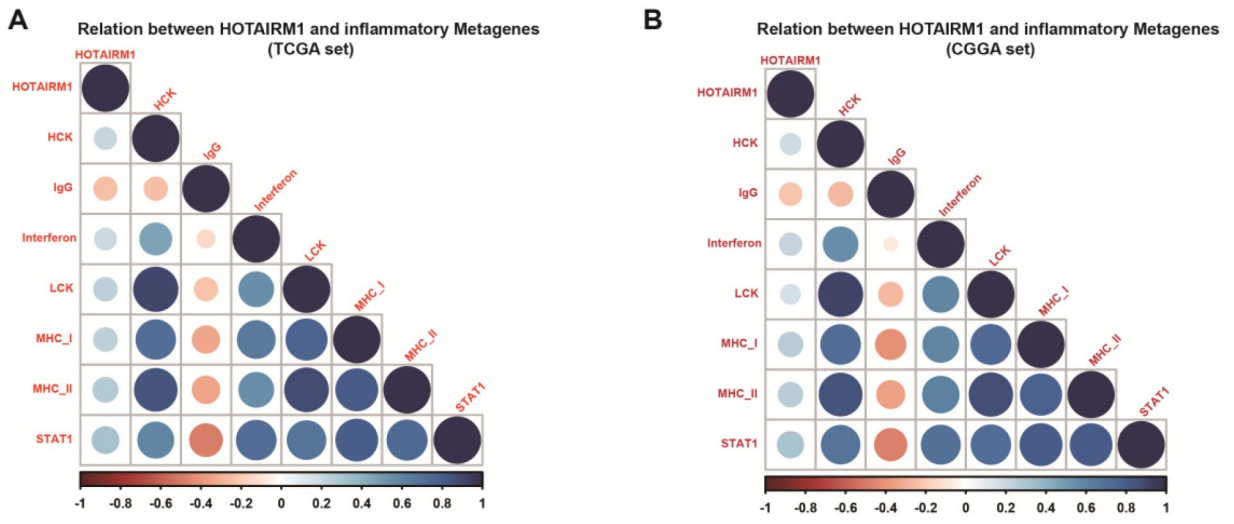

Supplementary Figure 9. HOTAIRM1 was associated with the regulation of inflammatory activities. Effect of HOTAIRM1 on inflammatory activities in TCGA (**A**) and CGGA (**B**) was assessed by Pearson correlation analysis.

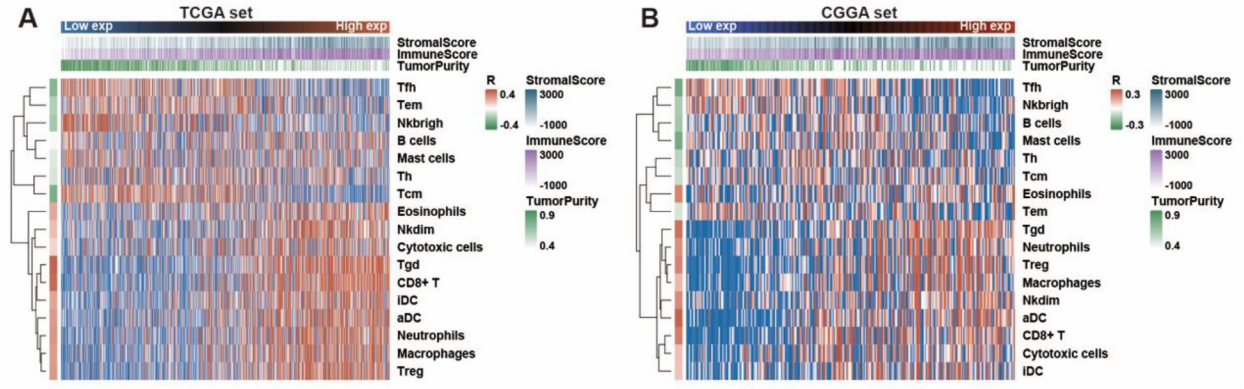

Supplementary Figure 10. HOTAIRM1 was associated with the regulation of the tumor microenvironment (TME). (**A**, **B**) High HOTAIRM1 expression was closely associated with low purity and immune cells including Gamma delta T cells (Tgd), CD8+ T cells, activated dendritic cells (aDC), and Regulatory T cells (Treg).

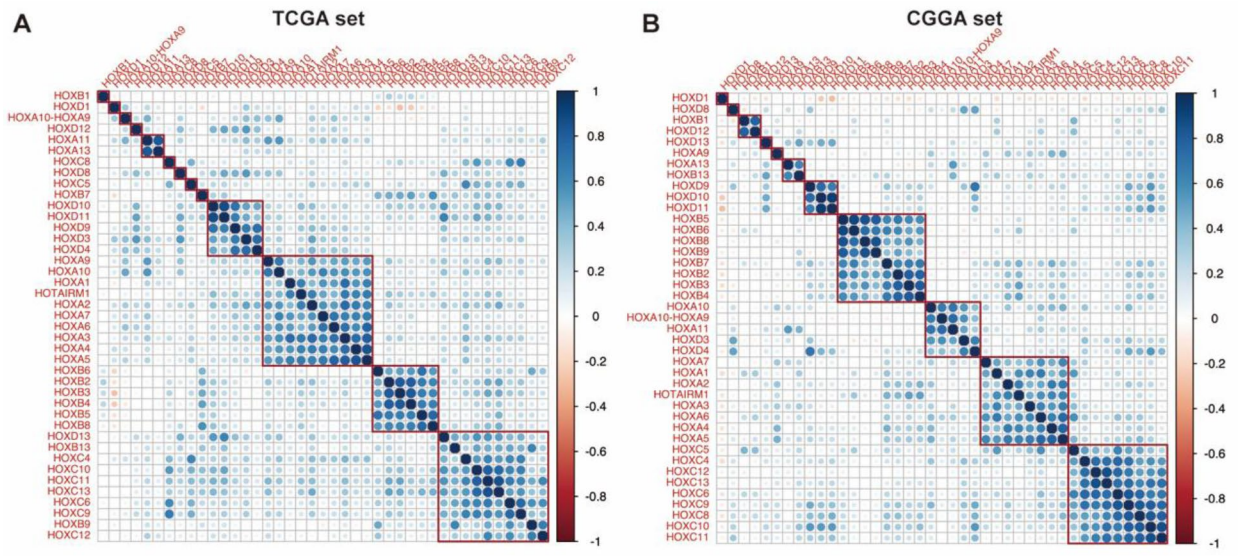

Supplementary Figure 11. HOTAIRM1 is positively associated with the HOXA gene family. (**A**, **B**) The relation between HOTAIRM1 and HOX gene family was investigated by Pearson's correlation analysis.

Supplementary Tables

Supplementary Table 1. Clinical and molecular information of glioma samples from TCGA and CGGA set included in this study.

	TCGA set (N = 672)	CGGA set (N = 274)
Age, years		
Mean (range)	46.86 (14-89)	42.92 (8-81)
Gender		
Female	284 (42.3%)	105 (38.3%)
Male	386 (57.4%)	169 (61.7%)
Unavailable	2 (0.3%)	0 (0.0%)
KPS		
Mean (range)	83.52 (40-100)	Unavailable
WHO grade		
Grade II	216 (32.1%)	101 (36.9%)
Grade III	237 (35.3%)	72 (26.3%)
Grade IV	160 (23.8%)	101 (36.9%)
Unavailable	59 (8.8%)	0 (0.0%)
Histopathology		
Oligodendroglioma	190 (28.3%)	34 (12.4%)
Oligoastrocytoma	128 (19.0%)	72 (26.3%)
Astrocytoma	192 (28.6%)	67 (24.5%)
Glioblastoma	160 (23.8%)	101 (36.9%)
Unavailable	2 (0.3%)	0 (0.0%)
Molecular classification		
LGG-Oligo	175 (26.0%)	0 (0.0%)
LGG-Astro	239 (35.6%)	0 (0.0%)
LGG-IDHwt	94 (14.0%)	48 (17.5%)
GBM-IDHmut	11 (1.6%)	27 (9.9%)
GBM-IDHwt	143 (21.3%)	74 (27.0%)
Unavailable	10 (1.5%)	125 (45.6%)
TCGA subtype		
Classical	214 (31.8%)	55 (20.1%)
Mesenchymal	59 (8.8%)	54 (19.7%)
Neural	28 (4.2%)	74 (27.0%)
Proneural	371 (55.2%)	91 (33.2%)
IDH status		
Mutant	425 (63.2%)	152 (55.5%)
Wild-type	238 (35.4%)	122 (44.5%)
Unavailable	9 (1.3%)	0 (0.0%)
1p19q status		
codel	168 (25.0%)	0 (0.0%)
non-codel	498 (74.1%)	0 (0.0%)
Unavailable	6 (0.9%)	274 (100.0%)
Chr7 gain/Chr10 loss		
YES	156 (23.2%)	0 (0.0%)
NO	507 (75.4%)	0 (0.0%)
Unavailable	9 (1.3%)	274 (100.0%)
MGMT promoter status		
Methylated	474 (70.5%)	0 (0.0%)
Unmethylated	164 (24.4%)	0 (0.0%)
Unavailable	34 (5.1%)	274 (100.0%)

TERT promoter status		
Mutant	157 (23.4%)	0 (0.0%)
Wild-type	163 (24.3%)	0 (0.0%)
Unavailable	352 (52.4%)	274 (100.0%)
PTEN status		
Mutant	64 (9.5%)	13 (4.7%)
Wild-type	588 (87.5%)	74 (27.0%)
Unavailable	20 (3.0%)	187 (68.2%)
ATRX status		
Mutant	195 (29.0%)	30 (10.9%)
Wild-type	463 (68.9%)	244 (89.1%)
Unavailable	14 (2.1%)	0 (0.0%)
TP53 status		
Mutant	280 (41.7%)	163 (59.5%)
Wild-type	372 (55.4%)	111 (40.5%)
Unavailable	20 (3.0%)	0 (0.0%)
EGFR status		
Mutant	66 (9.8%)	100 (36.5%)
Wild-type	586 (87.2%)	174 (63.5%)
Unavailable	20 (3.0%)	0 (0.0%)
Radiotherapy		
YES	413 (61.5%)	183 (66.8%)
NO	198 (29.5%)	72 (26.3%)
Unavailable	61 (9.1%)	19 (6.9%)
Chemotherapy		
YES	344 (51.2%)	135 (49.3%)
NO	52 (7.7%)	113 (41.2%)
Unavailable	276 (41.1%)	26 (9.5%)
Overall survival, months		
Median	29.3	43.2
Survival status		
Alive	248 (36.9%)	118 (43.1%)
Dead	417 (62.1%)	141 (51.5%)
Unavailable	7 (1.0%)	15 (5.5%)

Supplementary Table 2. The primers and microRNA assays in this study.

Primer name	Primer sequence (5'-3') or assay ID
HOTAIRM1 Fwd	CTGGCGAGAGGTCTGTTTTG
HOTAIRM1 Rev	AACACCCACATTTCAACCCC
FOXA1 Fwd	GCAATACTCGCCTTACGGCT
FOXA1 Rev	TACACACCTTGGTAGTACGCC
COL1A1 Fwd	GAGGGCCAAGACGAAGACATC
COL1A1 Rev	CAGATCACGTCATCGCACAAC
COL3A1 Fwd	TTGAAGGAGGATGTTCCCATCT
COL3A1 Rev	ACAGACACATATTTGGCATGGTT
COL8A1 Fwd	GGGAGTGCTGCTTACCATTTC
COL8A1 Rev	AGCGGCTTGATCCCATAGTAG
GPX8 Fwd	TACTTAGGGCTGAAGGAACTGC
GPX8 Rev	GGCTCCGATTCTCCAAACTGA
SOD2 Fwd	GCTCCGGTTTTGGGGTATCTG
SOD2 Rev	GCGTTGATGTGAGGTTCCAG
COL5A1 Fwd	TACAACGAGCAGGGTATCCAG
COL5A1 Rev	ACTTGCCATCTGACAGGTTGA
FGF7 Fwd	TCCTGCCAACTTTGCTCTACA
FGF7 Rev	CAGGGCTGGAACAGTTCACAT
IGFBP3 Fwd	AGACACACTGAATCACCTGAAGT
IGFBP3 Rev	AGGGCGACACTGCTTTTTCTT
COL1A2 Fwd	GAGCGGTAACAAGGGTGAGC
COL1A2 Rev	CTTCCCCATTAGGGCCTCTC
SPP1 Fwd	GCCGAGGTGATAGTGTGGTT
SPP1 Rev	AACGGGGATGGCCTTGTATG
COL4A1 Fwd	GGACTACCTGGAACAAAAGGG
COL4A1 Rev	GCCAAGTATCTCACCTGGATCA
POTEE Fwd	TGGATGATGATACCGCCGTG
POTEE Rev	TCCCAGTTGGTGATGATGCC
IL1B Fwd	ATGATGGCTTATTACAGTGGCAA
IL1B Rev	GTCGGAGATTCGTAGCTGGA
IL6 Fwd	ACTCACCTCTTCAGAACGAATTG
IL6 Rev	CCATCTTTGGAAGGTTCAGGTTG
TGFB1 Fwd	CTAATGGTGGAAACCCACAACG
TGFB1 Rev	TATCGCCAGGAATTGTTGCTG
PTGS2 Fwd	TAAGTGCGATTGTACCCGGAC
PTGS2 Rev	TTTGTAGCCATAGTCAGCATTGT
STAT3 Fwd	ACCAGCAGTATAGCCGCTTC
STAT3 Rev	GCCACAATCCGGGCAATCT
CCL2 Fwd	CAGCCAGATGCAATCAATGCC
CCL2 Rev	TGGAATCCTGAACCCACTTCT
18S Fwd	GCAGAATCCACGCCAGTACAAGAT
18S Rev	TCTTCTTCAGTCGCTCCAGGTCTT
hsa-miR-129-5p	Assay ID: 002298
hsa-miR-495-3p	Assay ID: 001663
U6	Assay ID: 001093

Supplementary Table 3. The distribution of clinical and molecular features between high-exp group and low-exp group.

	TCGA set			CGGA set		
	High-exp group (N = 336)	Low-exp group (N = 336)	P value	High-exp group (N = 137)	Low-exp group (N = 137)	P value
Age, years			<0.0001			<0.0001
Mean (range)	52.79 (21-89)	40.89 (14-75)		46.36 (8-81)	39.49 (10-	
Gender			0.0623			0.2140
Female	130 (38.7%)	154 (45.8%)		47 (34.3%)	58 (42.3%)	
Male	206 (61.3%)	180 (53.6%)		90 (65.7%)	79 (57.7%)	
Unavailable	0 (0.0%)	2 (0.6%)		0 (0.0%)	0 (0.0%)	
KPS			<0.0001			Unavailable
Mean (range)	79.61 (40-100)	88.31 (40-90)		Unavailable	Unavailable	
WHO grade			<0.0001			<0.0001
Grade II	45 (13.4%)	171 (50.9%)		25 (18.2%)	76 (55.5%)	
Grade III	110 (32.7%)	127 (37.8%)		34 (24.8%)	38 (27.7%)	
Grade IV	152 (45.2%)	8 (2.4%)		78 (56.9%)	23 (16.8%)	
Unavailable	29 (8.6%)	30 (8.9%)		0 (0.0%)	0 (0.0%)	
Histopathology			<0.0001			<0.0001
Oligodendroglio	44 (13.1%)	146 (43.5%)		6 (4.4%)	28 (20.4%)	
Oligoastrocytoma	44 (13.1%)	84 (25.0%)		24 (17.5%)	48 (35.0%)	
Astrocytoma	96 (28.6%)	96 (28.6%)		29 (21.2%)	38 (27.7%)	
Glioblastoma	152 (45.2%)	8 (2.4%)		78 (56.9%)	23 (16.8%)	
Unavailable	0 (0.0%)	2 (0.6%)		0 (0.0%)	0 (0.0%)	
Molecular			<0.0001			0.0003
LGG-Oligo	35 (10.4%)	140 (41.7%)		0 (0.0%)	0 (0.0%)	
LGG-Astro	73 (21.7%)	166 (49.4%)		0 (0.0%)	0 (0.0%)	
LGG-IDHwt	75 (22.3%)	19 (5.7%)		29 (21.2%)	19 (13.9%)	
GBM-IDHmut	7 (2.1%)	4 (1.2%)		14 (10.2%)	13 (9.5%)	
GBM-IDHwt	140 (41.7%)	3 (0.9%)		64 (46.7%)	10 (7.3%)	
Unavailable	6 (1.8%)	4 (1.2%)		30 (21.9%)	95 (69.3%)	
TCGA subtype			<0.0001			<0.0001
Classical	153 (45.5%)	61 (18.2%)		41 (29.9%)	14 (10.2%)	
Mesenchymal	57 (17.0%)	2 (0.6%)		49 (35.8%)	5 (3.6%)	
Neural	26 (7.7%)	2 (0.6%)		18 (13.1%)	56 (40.9%)	
Proneural	100 (29.8%)	271 (80.7%)		29 (21.2%)	62 (45.3%)	
IDH status			<0.0001			<0.0001
Mutant	115 (34.2%)	310 (92.3%)		44 (32.1%)	108 (78.8%)	
Wild-type	215 (64.0%)	23 (6.8%)		93 (67.9%)	29 (21.2%)	
Unavailable	6 (1.8%)	3 (0.9%)		0(0.0%)	0(0.0%)	
1p19q status			<0.0001			Unavailable
codel	33 (9.8%)	135 (40.2%)		0 (0.0%)	0 (0.0%)	
non-codel	298 (88.7%)	200 (59.5%)		0 (0.0%)	0 (0.0%)	
Unavailable	5 (1.5%)	1 (0.3%)		137 (100.0%)	137	
Chr7 gain/Chr10			<0.0001			Unavailable
YES	150 (44.6%)	6 (1.8%)		0 (0.0%)	0 (0.0%)	
NO	181 (53.9%)	326 (97.0%)		0 (0.0%)	0 (0.0%)	
Unavailable	5 (1.5%)	4 (1.2%)		137 (100.0%)	137	
MGMT promoter			<0.0001			Unavailable
Methylated	179 (53.3%)	295 (87.8%)		0 (0.0%)	0 (0.0%)	
Unmethylated	125 (37.2%)	39 (11.6%)		0 (0.0%)	0 (0.0%)	

Unavailable	32 (9.5%)	2 (0.6%)		137 (100.0%)	137	
TERT promoter			0.0025			Unavailable
Mutant	75 (22.3%)	82 (24.4%)		0 (0.0%)	0 (0.0%)	
Wild-type	50 (14.9%)	113 (33.6%)		0 (0.0%)	0 (0.0%)	
Unavailable	211 (62.8%)	141 (42.0%)		137 (100.0%)	137	
PTEN status			<0.0001			0.0352
Mutant	60 (17.9%)	4 (1.2%)		11 (8.0%)	2 (1.5%)	
Wild-type	265 (78.9%)	323 (96.1%)		35 (25.5%)	39 (28.5%)	
Unavailable	11 (3.3%)	9 (2.7%)		91 (66.4%)	96 (70.1%)	
ATRX status			<0.0001			0.8466
Mutant	68 (20.2%)	127 (37.8%)		16 (11.7%)	14 (10.2%)	
Wild-type	257 (76.5%)	206 (61.3%)		121 (88.3%)	123 (89.8%)	
Unavailable	11 (3.3%)	3 (0.9%)		0 (0.0%)	0 (0.0%)	
TP53 status			0.0260			0.0850
Mutant	125 (37.2%)	155 (46.1%)		89 (65.0%)	74 (54.0%)	
Wild-type	200 (59.5%)	172 (51.2%)		48 (35.0%)	63 (46.0%)	
Unavailable	11 (3.3%)	9 (2.7%)		0 (0.0%)	0 (0.0%)	
EGFR status			<0.0001			0.2587
Mutant	61 (18.2%)	5 (1.5%)		45 (32.8%)	55 (40.1%)	
Wild-type	264 (78.6%)	322 (95.8%)		92 (67.2%)	82 (59.9%)	
Unavailable	11 (3.3%)	9 (2.7%)		0 (0.0%)	0 (0.0%)	
Radiotherapy			<0.0001			0.8867
YES	242 (72.0%)	171 (50.9%)		90 (65.7%)	93 (67.9%)	
NO	66 (19.6%)	132 (39.3%)		34 (24.8%)	38 (27.7%)	
Unavailable	28 (8.3%)	33 (9.8%)		13 (9.5%)	6 (4.4%)	
Chemotherapy			0.0080			0.0054
YES	187 (55.7%)	157 (46.7%)		75 (54.7%)	60 (43.8%)	
NO	39 (11.6%)	13 (3.9%)		48 (35.0%)	65 (47.4%)	
Unavailable	110 (32.7%)	166 (49.4%)		14 (10.2%)	12 (8.8%)	

For category features we used chi-square or Fisher's exact test. For continuous features we calculate p value by Student's t test.

Supplementary Table 4. The distribution features of HOTAIRM1 expression level in various glioma subtypes.

	TCGA set		CGGA set	
	Expression level of HOTAIRM1 (mean (sd))	P value	Expression level of HOTAIRM1 (mean (sd))	Pvalue
WHO grade		<0.0001		<0.0001
Grade II	0.45 (0.54)		0.50 (0.55)	
Grade III	1.00 (1.13)		1.14 (1.25)	
Grade IV	2.44 (1.15)		1.77 (1.15)	
Histopathology		<0.0001		<0.0001
Oligodendroglioma	0.52 (0.73)		0.37 (0.41)	
Oligoastrocytoma	0.65 (0.77)		0.78 (1.05)	
Astrocytoma	1.07 (1.18)		0.95 (1.00)	
Glioblastoma	2.44 (1.15)		1.77 (1.15)	
Molecular classification		<0.0001		0.0009
LGG-Oligo	0.40 (0.49)		Unavailable	
LGG-Astro	0.52 (0.47)		Unavailable	
LGG-IDHwt	2.03 (1.41)		1.38 (1.37)	
GBM-IDHmut	1.61 (1.03)		1.12 (0.96)	
GBM-IDHwt	2.52 (1.13)		2.01 (1.12)	
TCGA subtype		<0.0001		<0.0001
Proneural	0.63 (0.88)		0.70 (0.79)	
Classical	1.61 (1.33)		2.06 (1.47)	
Neural	2.44 (1.24)		0.55 (0.60)	
Mesenchymal	2.26 (0.99)		1.75 (0.92)	

P value was calculated by one-way ANOVA.

Supplementary Table 5. IC50 of TMZ in si-NC or si-HOTAIRM1 group.

	IC50 (μM) (U87)	IC50 (μM) (LN229)
si-NC	494.1	1367
si-HOTAIRM1-1	220.8	629.5
si-HOTAIRM1-2	200.7	751.3

Please browse Full Text version to see the data of Supplementary Datasets 1–3:

Supplementary Datasets 1. Differentially upregulated genes in high-exp group compared with low-exp group.

Supplementary Datasets 2. Differentially downregulated miRNAs (down-DE miRNAs) in glioblastoma (GBM) compared with normal brain tissue.

Supplementary Datasets 3. Gene set on activation of immune response, T cell-mediated immune response and immune response to tumor cell.